Advanced Course and Workshop on Blood Flow
BF 2005 – (pp.309–359) – Warsaw, 2005.

Geometrical Multiscale Models for the Cardiovascular System

Luca Formaggia and Alessandro Veneziani

MOX—Modeling and Scientific Computing
Department of Mathematics "F. Brioschi"
Politecnico di Milano Piazza L. da Vinci 32, 20133 Milan, Italy
alessandro.veneziani@mate.polimi.it

These notes address the set up of mathematical and numerical models for the cardiovascular system and the numerical coupling of models having a different level of detail (from 3D down to lumped paramaters models), in what has been called the "geometrical multiscale approach". We present at first the basic features of reduced (1D and lumped parameter) models for the cardiovascular network. Then we address both mathematical and numerical issues arising when coupling models with a different level of detail. Finally, we present some numerical results.

Key words: *Blood flow problems, heterogeneous modeling, multiscale techniques*

1. Introduction

One of the major difficulties encountered when modeling in an accurate way the human cardiovascular system is that it is in fact formed by a closed network with a high level of inter-dependency. The flow dynamics of the blood in a specific vascular district (*local haemodynamics*) is strictly related to the global, systemic dynamics. For instance, the distribution of blood flow inside the various vascular districts, which is a systemic feature, influences for the blood dynamics in each district (local feature). Besides, the study of local flow feature is important since pathologies like the formation of local intimal thickening or plaques is strongly influenced by the local hemodynamics (see e.g. [68]). On the other hand, *local* alteration in vascular lumen induces a *global redistribution of the blood flow*, giving rise to compensatory mechanisms that, at some extents, can ensure a sufficient blood flow in the districts downstream the stenosis. Neglecting such effect provides only a partial infor-

mation (see e.g. [3, 5]). This reciprocal influence between local and systemic hemodynamics has led to the concept of *geometrical "multiscale"* modelling of the circulation Actually, the term "multiscale" is often used with different meanings in different fields of mathematical and numerical modelling. (e.g. wavelets, turbulence modelling etc.). Therefore, in order to avoid ambiguities, we indicate by the term *geometrical* our present multiscale perspective. In fact, this feature is common to all many problems involving modeling subregions of a larger and complex system, such as hydraulic or electric networks. Examples are the simulation of exhaust systems of Diesel engines (see [13]), and the design of electric circuits (see [4]).

A multiscale perspective is relevant even when one is interested just on the description of the local flow. Indeed, the formulation of a mathematical well posed problem requires the specification of boundary data (see [61]). The vascular walls are physical boundaries and the correct conditions are suggested by physical assumptions such as the continuity of the velocity field. However, *artificial boundaries* have to be introduced to bound the vascular district at hand. They are the interface between the district under consideration and the remainder of the circulatory system. Boundary conditions on such boundaries are, in fact, influenced by the "multiscale" nature of the circulation. Whenever such data are not available from specific (and accurate!) measurements, a proper boundary condition would require a mathematical description of the action of the circulatory system on the vascular district at hand. Clearly, since it is not affordable to describe the whole circulatory system at the same level of detail, this mathematical description must rely on simpler models.

While the local model will be typically based on the solution of the incompressible Navier-Stokes possibly coupled with the dynamics of the vessel walls (see e.g. [1, 46]), the systemic model will be given by *1D models* or by *lumped parameters* models based on the solution of a system of ordinary differential equation (in time) for the average mass flow and pressure in the different compartments forming the cardiovascular system.

Besides their intrinsic relevance, these "simple-minded" models are of great interest in our multiscale perspective. Indeed, they provide a systemic description of the main phenomena related to the circulation (such as the compensatory mechanisms mentioned above) at a low computational cost. They may thus be coupled with an accurate (but local) description of a vascular district of interest. The mathematical and numerical issues related to

this coupling are nontrivial. The different level of detail of the different models is reflected by different mathematical features. Navier-Stokes equations are a system of non-linear partial differential equations which are essentially parabolic for the velocity, while the 1D models are (mainly) based on hyperbolic partial differential equations, and the lumped parameter models do not feature a spatial dependency and are described by means of ordinary differential equations in the time variable (for this reason, they are also called "0D models"). A particular care has therefore to be taken in managing the interfaces between these models in order to have mathematically well posed problems and to guarantee accurate numerical results.

In these notes, we will start with a short introduction of simple-minded models for the circulation. We will consider 1D models at first (Section 2), their derivation and their numerical treatment. We will also briefly address some specific issue such as the 1D modeling of curved pipes. Then, we will introduce lumped parameter models (Section 3), their basic features and the set up of systemic models. The specific mathematical and numerical problems arising in the coupling of these models are addressed in Sections 4 and 5. Numerical results are finally presented in Sec. 6, illustrating the effectiveness of the multiscale approach not only for academic test cases but also in simulations of real medical interest.

2. The Basic 1D Model

We introduce the simplest non-linear 1D model for blood flow in compliant vessels. For more details, see [1] or [3].

The basic equations are derived for a tract of artery free of bifurcations, which is idealised as a cylindrical compliant tube (see Fig. 1). We will denote by $I = (t_0, t_1)$ the time interval of interest and for the sake of convenience we will take $t_0 = 0$. By Ω_t we indicate the spatial domain which is supposed to be a circular cylinder filled with blood, which is changing with time under the action of the pulsatile fluid.

We will mainly use Cartesian coordinates, yet when dealing with cylindrical geometries it is handy to introduce a cylindrical coordinate system. Therefore, in the following we indicate with $\mathbf{e}_r$, $\mathbf{e}_\theta$ and $\mathbf{e}_z$ the radial, circumferential and axial unit vectors, respectively, (r, θ, z) being the corresponding coordinates. We assume that the vessel extends from $z = 0$ to $z = l$ and the vessel length l is constant with time.

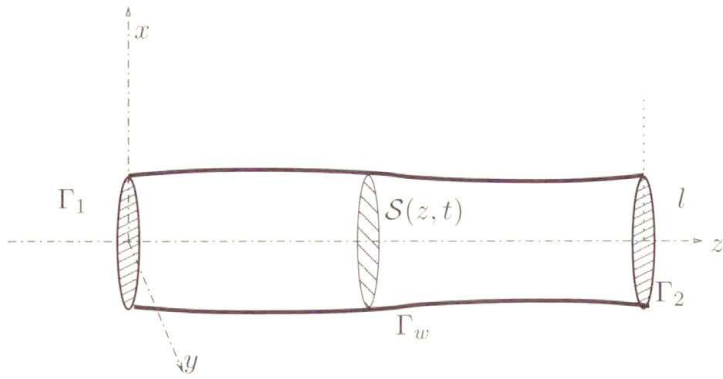

FIGURE 1. Simplified geometry. The vessel is assumed to by a straight cylinder with circular cross section.

The basic model is deduced by making the following simplifying assumptions.

A.1. *Axial symmetry.* All quantities are independent from the angular coordinate θ. As a consequence, every axial section z =const remains circular during the wall motion. The tube radius R is a function of z and t.

A.2. *Radial displacements.* The wall displaces along the radial direction solely, thus at each point on the tube surface we may write $\boldsymbol{\eta} = \eta \mathbf{e}_r$, where $\eta = R - R_0$ is the displacement with respect to the reference radius R_0.

A.3. *Fixed rectilinear cylindrical vessels.* This simply means that the vessel will expand and contract around its axis, which is fixed in time.

A.4. *Constant pressure on each axial section.* We assume that the pressure P is constant on each section, so that it depends only on z and t.

A.5. *No body forces.*

A.6. *Dominance of axial velocity.* The velocity components orthogonal to the z axis are negligible compared to the component along z. The latter is indicated by u_z and its expression in cylindrical coordinates is supposed to be of the form

$$u_z(t, r, z) = \overline{u}(t, z)\varphi\left(rR^{-1}(z)\right) \tag{2.1}$$

where $\overline{u}$ is the *mean velocity* on each axial section and $\varphi : \mathbb{R} \to \mathbb{R}$ is a *velocity profile*. The fact that the velocity profile does not vary in time and space is in contrast with experimental observations and numerical results carried out with full scale models. However, it is a necessary assumption for the derivation of the reduced model. One may then think φ as being a profile representative of an average flow configuration.

A generic axial section will be indicated by $\mathcal{S} = \mathcal{S}(t, z)$. Its measure A is given by

$$A(t, z) = \int_{\mathcal{S}(t,z)} d\sigma = \pi R^2(t, z) = \pi(R_0(z) + \eta(t, z))^2. \tag{2.2}$$

The mean velocity $\overline{u}$ is then given by $\overline{u} = A^{-1} \int_{\mathcal{S}} u_z d\sigma$, and from (2.1) it follows easily that φ must be such that

$$\int_0^1 \varphi(y) y dy = \frac{1}{2}$$

We will indicate with α the *momentum-flux correction coefficient*, (sometimes also called *Coriolis coefficient*) defined as

$$\alpha = \frac{\int_{\mathcal{S}} {u_z}^2 d\sigma}{A\overline{u}^2} = \frac{\int_{\mathcal{S}} \varphi^2 d\sigma}{A}, \tag{2.3}$$

where the dependence of the various quantities on the spatial and time coordinates is understood. It is possible to verify that $\alpha \geq 1$. In general this coefficient will vary in time and space, yet in our model it is taken constant as a consequence of (2.1).

A possible choice for the profile law is the parabolic profile $\varphi(y) = 2(1 - y^2)$ that corresponds to the well known Poiseuille solution characteristic of steady flows in circular tubes. In this case we have $\alpha = 4/3$. However, for blood flow in arteries it has been found that the velocity profile is, on average, rather flat. Indeed, a profile law often used for blood flow in arteries (see for instance [56]) is a power law of the type $\varphi(y) = \gamma^{-1}(\gamma + 2)(1 - y^\gamma)$ with typically $\gamma = 9$. Correspondingly, we have $\alpha = (\gamma + 2)/(\gamma + 1) = 1.1$. The choice $\alpha = 1$, which indicates a completely flat velocity profile, simplifies the analysis, so it is quite often adopted.

The mean flux Q, defined as $Q = \int_{\mathcal{S}} u_z d\sigma = A\overline{u}$, is one of the main variables of our problem, together with A and the pressure P.

There are (at least) three ways of deriving a 1D model for an incompressible fluid filling a compliant pipe. The first one moves from the incompressible Navier-Stokes equations and performs an asymptotic analysis by assuming that the ratio R_0/L is small, thus discarding the higher order terms with respect to R_0/L, [7]. The second approach derives the model directly from the basic conservation laws written in integral form. The third approach consists of integrating the Navier-Stokes equations on a generic section $\mathcal{S}$.

Following the last approach and exploting the assumptions stated above, it is possible to obtain the following system of equations (see [1, 3]): for $z \in (0, L)$ and $t \in I$

$$\begin{cases} \dfrac{\partial A}{\partial t} + \dfrac{\partial Q}{\partial z} = 0, \\ \dfrac{\partial Q}{\partial t} + \alpha \dfrac{\partial}{\partial z}\left(\dfrac{Q^2}{A}\right) + \dfrac{A}{\rho}\dfrac{\partial P}{\partial z} + K_r\left(\dfrac{Q}{A}\right) = 0, \end{cases} \tag{2.4}$$

where the unknowns are A, Q and P and α is here taken constant, and K_r is a coefficient proportional to the blood viscosity.

In order to close system (2.4), where three unknowns, P, A and Q are related by two equations, we have to provide a relation for the pressure. A complete mechanical model for the structure of the vessel wall would provide a differential equation which links the displacement and its spatial and temporal derivatives to the force applied by the fluid. Here we will adopt instead an hypothesis quite commonly used in practice, namely, that the inertial terms are neglegible and that the elastic stresses in the circumferential direction are dominant. Under these assumptions, the wall mechanics reduces to an algebraic relation linking pressure to the wall deformation and consequently to the vessel section A. Actually, we may assume that the pressure satisfies a relation like

$$P(t, z) - P_{ext} = \psi(A(t, z); A_0(z), \boldsymbol{\beta}(z)), \tag{2.5}$$

where we have outlined that the pressure will in general depend also on $A_0 = \pi R_0^2$ and on a set of coefficients $\boldsymbol{\beta} = (\beta_0, \beta_1, \cdots, \beta_p)$, related to physical and mechanical properties, that are, in general, *given* functions of z (see [1]). Here P_{ext} indicates the external pressure exerted by the organs outside the vessel (often taken equal to 0). For instance, by exploiting the well known linear elastic law for a cylindrical vessel and using the fact that

$$\eta = (\sqrt{A} - \sqrt{A_0})/\sqrt{\pi} \tag{2.6}$$

we can obtain the following expression for ψ

$$\psi(A; A_0, \beta_0) = \beta_0 \frac{\sqrt{A} - \sqrt{A_0}}{A_0}. \tag{2.7}$$

We have identified $\boldsymbol{\beta}$ with the single parameter β_0 that from the modelling assumptions is $= (\sqrt{\pi} h_0 E)/(1 - \xi^2)$ (see however the next remark for the numerical estimate of β_0). The algebraic relation (2.5) assumes that the wall is instantaneously in equilibrium with the pressure forces acting on it (see for instance [1] or [46]). More sophisticated models may be introduced by employing a differential law for the vessel structure, including the inertia and the viscoelasticity of the wall: the interested reader is referred to [1].

By exploiting relation (2.5) we may eliminate the pressure P from the momentum equation. To that purpose we will indicate by $c_1 = c_1(A; A_0, \boldsymbol{\beta})$ the following quantity

$$c_1 = \sqrt{\frac{A}{\rho} \frac{\partial \psi}{\partial A}}, \tag{2.8}$$

which has the dimension of a velocity and, as we will see later on, is related to the speed of propagation of simple waves along the tube.

By simple manipulations (2.4) may be written in *quasi-linear* form as follows

$$\frac{\partial}{\partial t}\mathbf{U} + \mathrm{H}(\mathbf{U}) \frac{\partial \mathbf{U}}{\partial z} + \mathrm{B}(\mathbf{U}) = \mathbf{0}, \tag{2.9}$$

where,

$$\mathbf{U} = \begin{bmatrix} A \\ Q \end{bmatrix},$$

$$\mathrm{H}(\mathbf{U}) = \begin{bmatrix} 0 & 1 \\ \dfrac{A}{\rho} \dfrac{\partial \psi}{\partial A} - \alpha \overline{u}^2 & 2\alpha \overline{u} \end{bmatrix} = \begin{bmatrix} 0 & 1 \\ c_1^2 - \alpha \left(\dfrac{Q}{A} \right)^2 & 2\alpha \dfrac{Q}{A} \end{bmatrix}, \tag{2.10}$$

and

$$\mathrm{B}(\mathbf{U}) = \begin{bmatrix} 0 \\ K_R \left(\dfrac{Q}{A} \right) + \dfrac{A}{\rho} \dfrac{\partial \psi}{\partial A_0} \dfrac{dA_0}{dz} + \dfrac{A}{\rho} \dfrac{\partial \psi}{\partial \boldsymbol{\beta}} \dfrac{d\boldsymbol{\beta}}{dz} \end{bmatrix}.$$

A *conservation form* for (2.9) may be found as well and reads

$$\frac{\partial \mathbf{U}}{\partial t} + \frac{\partial}{\partial z}[F(\mathbf{U})] + \mathbf{B}(\mathbf{U}) = \mathbf{0}, \tag{2.11}$$

where

$$F(\mathbf{U}) = \begin{bmatrix} Q \\ \alpha \frac{Q^2}{A} + C_1 \end{bmatrix}, \quad \mathbf{B}(\mathbf{U}) = \mathrm{B}(\mathbf{U}) - \begin{bmatrix} 0 \\ \frac{\partial C_1}{\partial A_0}\frac{dA_0}{dz} + \frac{\partial C_1}{\partial \boldsymbol{\beta}}\frac{d\boldsymbol{\beta}}{dz} \end{bmatrix},$$

and C_1 is a primitive of c_1^2 with respect to A, given by

$$C_1(A; A_0, \boldsymbol{\beta}) = \int_{A_0}^{A} c_1^2(\tau; A_0, \boldsymbol{\beta})\, d\tau.$$

System (2.11) allows to identify the vector $\mathbf{U}$ as the the *conservation variables* of the problem.

In the case we use relation (2.7) we have

$$c_1 = \sqrt{\frac{\beta_0}{2\rho A_0}} A^{\frac{1}{4}}, \quad C_1 = \frac{\beta_0}{3\rho A_0} A^{\frac{3}{2}}. \tag{2.12}$$

It is possible to prove that if $A \geq 0$, the matrix H possesses two real eigenvalues. Furthermore, if $A > 0$ the two eigenvalues are distinct, that means that (2.9) is a *strictly hyperbolic* system of partial differential equations (for the proof, see e.g. [1]).

Remark 1. An energy analysis of system (2.11) is carried out in [15].

Remark 2. The coefficients of the 1D model obtained depend on physical parameters related to the physical properties of the blood and the vascular wall, namely α, β_0, K_r and A_0. The accurate estimation of these parameters is a non trivial task. In [33] a nonlinear least square approach is proposed for the parameters estimate based on experimental data. In particular, in this work the parameter β_0 is estimated starting from "synthetic" data given by 3D fluid-structure interaction simulations. Numerical results reported show that the parameter estimation can be significantly different from the values computed by analytical formulas such as $\beta_0 = (\sqrt{\pi} h_0 E)/(1 - \xi^2)$ based on the simplifying assumptions, yielding however numerical results closer to the 3D data.

Characteristics analysis

The hyperbolic nature of the problem at hand allows its reformulation in terms of ordinary differential equations. This reformulation is based on the

so-called *characteristic analysis* and can be useful in the numerical solution of the problem. We briefly address this topic here. For a more detailed analysis see [1].

Let $(\mathbf{l}_1, \mathbf{l}_2)$ and $(\mathbf{r}_1, \mathbf{r}_2)$ be two couples of left and right eigenvectors of the matrix H in (2.10), respectively. The matrices $\mathbf{L}$, $\mathbf{R}$ and $\mathbf{\Lambda}$ are defined as

$$\mathbf{L} = \begin{bmatrix} \mathbf{l}_1^T \\ \mathbf{l}_2^T \end{bmatrix}, \qquad \mathbf{R} = \begin{bmatrix} \mathbf{r}_1 & \mathbf{r}_2 \end{bmatrix}, \qquad \mathbf{\Lambda} = \operatorname{diag}(\lambda_1, \lambda_2) = \begin{bmatrix} \lambda_1 & 0 \\ 0 & \lambda_2 \end{bmatrix}. \tag{2.13}$$

Since right and left eigenvectors are mutually orthogonal, without loss of generality we choose them so that $\mathbf{LR} = \mathbf{I}$. Matrix H may then be decomposed as

$$\mathrm{H} = \mathbf{R}\mathbf{\Lambda}\mathbf{L}, \tag{2.14}$$

and system (2.9) written in the equivalent form

$$\mathbf{L}\frac{\partial \mathbf{U}}{\partial t} + \mathbf{\Lambda}\mathbf{L}\frac{\partial \mathbf{U}}{\partial z} + \mathbf{L}\mathrm{B}(\mathbf{U}) = \mathbf{0}, \quad z \in (0, L),\ t \in I. \tag{2.15}$$

If there exist two quantities W_1 and W_2 which satisfy

$$\frac{\partial W_1}{\partial U} = \mathbf{l}_1, \quad \frac{\partial W_2}{\partial U} = \mathbf{l}_2, \tag{2.16}$$

we will call them *characteristic variables* of the hyperbolic system. We point out that in the case where the coefficients A_0 and $\boldsymbol{\beta}$ are not constant, $\mathbf{W}_1$ and $\mathbf{W}_2$ are not autonomous functions of $\mathbf{U}$.

By setting $\mathbf{W} = [W_1, W_2]^T$ system (2.15) may be elaborated into

$$\frac{\partial \mathbf{W}}{\partial t} + \mathbf{\Lambda}\frac{\partial \mathbf{W}}{\partial z} + \mathrm{G} = \mathbf{0}, \tag{2.17}$$

where

$$\mathrm{G} = \mathbf{L}\mathrm{B} - \frac{\partial W}{\partial A_0}\frac{dA_0}{dz} - \frac{\partial W}{\partial \boldsymbol{\beta}}\frac{d\boldsymbol{\beta}}{dz}. \tag{2.18}$$

If we consider the *characteristic line* $y_i(t)$ which satisfies the differential equation

$$\frac{d}{dt}y_i(t) = \lambda_i(t, y_i(t)), \quad i = 1, 2 \tag{2.19}$$

then (2.17) may be rewritten as

$$\frac{d}{dt}W_i(t, y_i(t)) + G_i(W_1, W_2) = 0, \quad i = 1, 2 \tag{2.20}$$

where we have made evident the dependence of G_i on the characteristic variables.

Equations (2.19) and (2.20) represent a possible reformulation of the problem at hand in terms of ordinary differential equations for the characteristic variables W_i. The role of these variables is relevant both at the mathematical and numerical level (see [32, 24]), in particular in the prescription of the boundary conditions.

Boundary conditions

System (2.4) must be supplemented by proper boundary conditions. The number of conditions to apply at each end equals the number of characteristics entering the domain through that boundary. Since we are only considering sub-critical flows *we have to impose exactly one boundary condition at both* $z = 0$ *and* $z = L$. An important class of boundary conditions are the so-called *non-reflecting or 'absorbing'* ones. They allow the simple wave associated to the outgoing characteristic variable to exit the computational domain with no reflections. Following [60, 25] non-reflecting boundary conditions for one dimensional systems of non-linear hyperbolic equations in conservation form like (2.11) may be written as

$$\mathbf{l}_1 \cdot \left(\frac{\partial \mathbf{U}}{\partial t} + \mathbf{B}(\mathbf{U}) \right) = 0 \text{ at } z = 0, \quad \mathbf{l}_2 \cdot \left(\frac{\partial \mathbf{U}}{\partial t} + \mathbf{B}(\mathbf{U}) \right) = 0 \text{ at } z = l,$$

for all $t \in I$, which in fact, by defining $R_i = \mathbf{l}_i \mathbf{B}$, may be written in the form

$$\frac{\partial W_1}{\partial t} + R_1(W_1, W_2) = 0 \text{ at } z = 0, \quad \frac{\partial W_2}{\partial t} + R_2(W_1, W_2) = 0 \text{ at } z = l, \tag{2.21}$$

where we have put into evidence the possible dependence of R_1 and R_2 on W_1 and W_2 through the dependence of $\mathbf{B}$ on $\mathbf{U}$. Boundary conditions of this type are quite convenient at the outlet (distal) section, particularly whenever we have no better data to impose on that location.

At the inlet (proximal) section instead one usually desires to impose values of pressure or mass flux derived from measurements or other means. Let us suppose, without loss of generality, that $z = 0$ is an inlet section. Whenever an explicit formulation of the characteristic variables is available, the boundary condition may be expressed directly in terms of the entering characteristic variable W_1, i.e., for all $t \in I$

$$W_1(t) = g_1(t) \text{ at } z = 0, \tag{2.22}$$

g_1 being a given function. However, seldom one has directly the boundary datum in terms of the characteristic variable, since is normally given in terms of physical variables. In these cases, some specific techniques can be devised for recovering the characteristic variable form the physical data. For instance, if $A(t)$ is available at $z = 0$, one could formulate:

$$W_1(t) = W_1(A(t), W_2(t))$$

where W_2 is the outgoing characteristic variable that can obtained by *extrapolation*, moving backward in time along the characteristic line $y_2(t)$. More details about this approach can be found e.g. in [1].

2.1. Numerical Approximation

We will here consider the equations in conservation form (2.11) and the simple algebraic relationship (2.7).

There are many different schemes for the numerical simulation of this kind of problem: the interested reader is referred e.g. to [14, 32, 48]. Here, we adopt a second order Taylor-Galerkin scheme which might be seen as the finite element counterpart of the well known Lax-Wendroff scheme. It has been chosen for its excellent dispersion error characteristics and its simplicity of implementation.

The basic idea of the scheme is to exploit the Taylor expansion of the solution in time up to the second time derivative and then to use the equations of the problem (2.11) for replacing the time derivatives with space derivatives and terms of order zero. This yields a semi-discrete problem (continuous in space, discrete in time). The space discretization is then obtained with a Galerkin Finite Element approach. A complete description of the method applied to the problem at hand can be found in [1].

Using the abridged notations

$$\mathbf{F}_{LW}(\mathbf{U}) = \mathbf{F}(\mathbf{U}) - \frac{\Delta t}{2}\mathbf{H}(\mathbf{U})\mathbf{B}(\mathbf{U})$$

and

$$\mathbf{B}_{LW}(\mathbf{U}) = \mathbf{B}(\mathbf{U}) + \frac{\Delta t}{2}\mathbf{B}_{\mathbf{U}}(\mathbf{U})\mathbf{B}(\mathbf{U}),$$

the discretization of the problem reads: given $\mathbf{U}_h^0$ obtained by interpolation from the initial data, for $n \geq 0$, find $\mathbf{U}_h^{n+1} \in \mathbf{V}_h$ which $\forall \boldsymbol{\psi}_h \in \mathbf{V}_h^0$ satisfies

the following equations for the interior nodes

$$(\mathbf{U}_h^{n+1}, \boldsymbol{\psi}_h) = (\mathbf{U}_h^n, \boldsymbol{\psi}_h) + \Delta t \left(\mathbf{F}_{LW}(\mathbf{U}_h^n), \frac{d\boldsymbol{\psi}_h}{dz} \right) - \frac{\Delta t^2}{2} \left(\mathbf{B}_{\mathbf{U}}(\mathbf{U}_h^n) \frac{\partial \mathbf{F}(\mathbf{U}_h^n)}{\partial z}, \boldsymbol{\psi}_h \right) - \frac{\Delta t^2}{2} \left(\mathbf{H}(\mathbf{U}_h^n) \frac{\partial \mathbf{F}}{\partial z}(\mathbf{U}_h^n), \frac{d\boldsymbol{\psi}_h}{dz} \right) - \Delta t \left(\mathbf{B}_{LW}(\mathbf{U}_h^n), \boldsymbol{\psi}_h \right), \quad (2.23)$$

together with the relation for boundary nodes obtained from the boundary and compatibility conditions, as discussed in the sequel. Here $(\cdot, \cdot)$ stands for the usual L^2 scalar product. By taking $\boldsymbol{\psi}_h = [\psi_i, 0]^T$ and $\boldsymbol{\psi}_h = [0, \psi_i]^T$, for $i = 1, \ldots, N$ we obtain N discrete equations for continuity and momentum, respectively, for a total of $2(N+2)$ unknowns (A_i and Q_i for $i = 0, \ldots, N+1$).

The second order Taylor-Galerkin scheme (2.23) entails a CFL stability bound on the time step:

$$\Delta t \leq \frac{\sqrt{3}}{3} \min_{0 \leq i \leq N} \left[\frac{h_i}{\max_{k=i}^{i+1} (c_{\alpha,k} + |\overline{u}_k|)} \right], \quad (2.24)$$

where $c_{\alpha,i}$ and $\overline{u}_i$ here indicate the values of c_α and $\overline{u}$ at mesh node z_i, respectively.

2.1.1. Boundary and compatibility conditions. Formulation (2.23) provides the values only at internal nodes, since we have chosen the test functions $\boldsymbol{\psi}_h$ to be zero at the boundary. The values of the unknowns at the boundary nodes must be provided by the application of the *boundary* and *compatibility* conditions.

The boundary conditions previously discussed are not sufficient to close the problem *at numerical level* since they provide just two conditions, yet we need to find four additional relations. We want to stress that this problem is linked to the numerical scheme, not to the differential equations, which indeed only require one condition at each end (at least for the flow regime we are considering here). Without loss of generality, let us consider the boundary $z = 0$ (analogous consideration may be made at $z = L$). As we have seen, the boundary conditions will provide at each time step a relation of the type

$$\phi(A_0^{n+1}, Q_0^{n+1}) = q_0(t^{n+1}),$$

being q_0 the given boundary data. For instance, imposing the pressure would mean choosing $\phi(A,Q) = P = \psi(A; A_0(0), \beta(0))$, while imposing the mass flux would just mean $\phi(A,Q) = Q$. Finally, a non reflecting condition is obtained by $\phi(A,Q) = W_1(A,Q)$ and in this case q_0 is normally taken constant and equal to the value of W_1 at a reference state (typically $(A,Q) = (A_0, 0)$). Thus, in general ϕ is a non linear function.

This relation should be supplemented by a *compatibility condition*. In general, the compatibility conditions are obtained by projecting the equation along the eigenvectors corresponding to the characteristics that are exiting the domain. Therefore, we have to discretise the following set of equations at the two vessel ends [48]:

$$\mathbf{l}_2 \cdot \left(\frac{\partial}{\partial t}\mathbf{U} + \mathrm{H}\frac{\partial \mathbf{U}}{\partial z} + \mathrm{B}(\mathbf{U}) \right) = 0, \quad z = 0,\, t \in I, \tag{2.25a}$$

$$\mathbf{l}_1 \cdot \left(\frac{\partial}{\partial t}\mathbf{U} + \mathrm{H}\frac{\partial \mathbf{U}}{\partial z} + \mathrm{B}(\mathbf{U}) \right) = 0, \quad z = L,\, t \in I. \tag{2.25b}$$

There are different techniques for considering these conditions in the numerical scheme: the interested reader is referred to [1].

2.2. Network of 1D Models

The vascular system is in fact a network of vessels that branches repeatedly and a model of just an artery is of little use. A simple and effective idea is to describe the network by 'gluing' together one dimensional models. Yet, we need to find proper interface conditions (i.e. mathematically sound and easy to treat numerically). The technique may be adopted also in the case of abrupt changes of vessel characteristics (see [20]).

The flow in a bifurcation is intrinsically three dimensional; yet it may still be represented by means of a 1D model, following a domain decomposition approach, if one is not interested in the flow details inside the branch (see e.g. [42]). Figure 2 (left) shows a model for a bifurcation. We have simplified the real geometric structure by imposing that the bifurcation is located exactly on one point and neglecting the effect of the bifurcation angles. An alternative technique is reported in [57], where a separate tract containing the branch is introduced.

In order to solve the three problems in Ω_1 (main branch), Ω_2 and Ω_3 we need to find appropriate interface conditions. The hyperbolic nature of the problem tells us that we need three conditions.

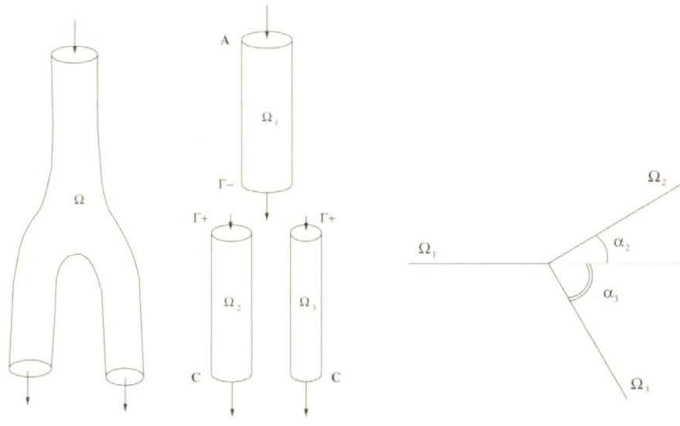

FIGURE 2. Left: One dimensional model of bifurcation by domain decomposition technique. Right:A sketch of a branching.

We first state the conservation of mass across the bifurcation, i.e.

$$Q_1 = Q_2 + Q_3, \quad \text{at } z = \Gamma, t \in I. \tag{2.26}$$

We note that the orientation of the axis in the three branches is such that a positive value of Q_1 indicates that blood is flowing from the main branch Ω_1 into the other two. An energy analysis allows us to conclude that a proper interface condition would entail the condition $P_{t,1}Q_1 - P_{t,2}Q_2 - P_{t,3}Q_3 \geq 0$, where $P_t := P + 1/2\rho|\mathbf{u}|^2$ is the *total pressure*. It is expected that the complex flow in the bifurcation will cause an energy dissipation and consequently a decrease in the total pressure in the direction of the flow field across the bifurcation, and this loss should be related to the fluid velocity (or flow rate) and to the bifurcation angles. A possibility to account for this is to impose, at $z = \Gamma$, that

$$\begin{aligned} P_{t,1} - \text{sign}(\bar{u}_1) f_1(\bar{u}_1) &= P_{t,2} + \text{sign}(\bar{u}_2) f_2(\bar{u}_2, \alpha_2), \\ P_{t,1} - \text{sign}(\bar{u}_1) f_1(\bar{u}_1) &= P_{t,3} + \text{sign}(\bar{u}_3) f_3(\bar{u}_3, \alpha_3), \end{aligned} \tag{2.27}$$

where α_2 and α_3 are the angles of the branches Ω_2 and Ω_3 with respect to the main one (see Fig. 2 right); f_1, f_2 and f_3 are suitable positive functions and equal to zero when the first argument is zero.

In the numerical scheme, (2.26) and (2.27) will be complemented by three compatibility relations (see Sect. 2.1.1). We have thus a non linear system for the six unknowns A_i^{n+1}, Q_i^{n+1}, $i = 1, 2, 3$, at the interface location Γ, which can be solved by a Newton method.

2.3. Modeling of Curved Pipes

One of the most relevant assumptions in devising the basic 1D model is that the axis of the (cylindrical) vessel is rectilinear. Actually, if we remove this hypothesis, it is still possible to define a main flow direction in the domain, namely the curvilinear abscissa along the axis, and however the blood dynamics in the other directions is no longer negligible (secondary motion zones): for a detailed description of the fluid dynamics in this case, see [43]. Nevertheless, there are some vessels which are clearly curved (aorta, femoral arteries, etc.). For these vessels, the basic 1D model (2.4) can be considered only as a rough description, possibly introducing a subdivision into subsegments sufficienly short to be considered straight and connected one to the other with a suitable angle $\neq 0$ (see Fig. 3 left). Alternatively, here we would like to briefly address the definition of 1D models which are able to account for the effects of the transversal dynamics on the axial one, having the computational cost of the "simple-minded" model (2.4). The task is not easy, since we want to devise a sort of 1D models for the cheap description of a genuinely 3D dynamics, so we call these models "psychologically 1D".

Simplified models for curved pipes can be obtained for small curvatures of the vessels with a perturbation analysis of the rectilinear model (see [11]).

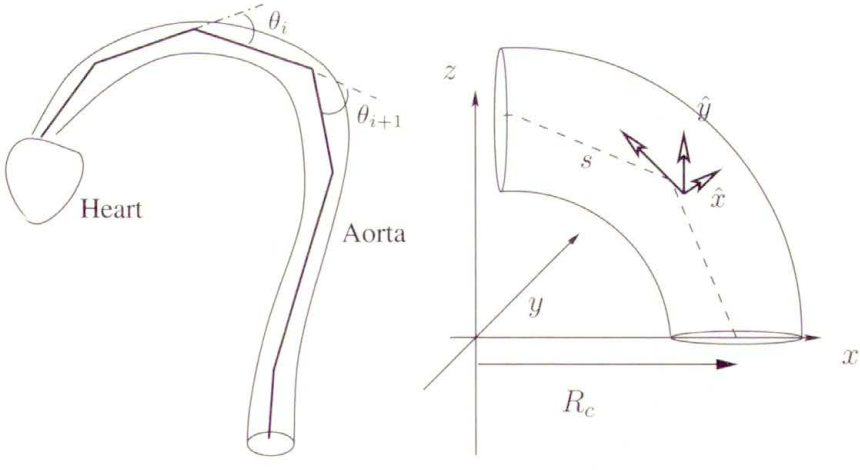

FIGURE 3. Left: Representation of a curved pipe as a set of straight cylinders. Right: Frame of reference for a planar curved pipe.

Let us consider the nondimensional parameter:

$$D = 2\sqrt{2}\sqrt{\frac{R_w}{R_c}}\mathrm{Re} \tag{2.28}$$

where R_w is the vessel radius, R_c is the curvature radius of the vessel axis ($R_c \to \infty$ in the straight case) and Re is the Reynolds number of the rectilinear case. D is called *Dean number*. Simplified models can be obtained for small values of the Dean number, which are for instance able to correctly compute the stagnation points of the secondary motion zones. For large values of D these models need to be suitably corrected, and the analysis becomes by far more difficult: a complete description of this approach can be found in [43], Chap. 4. A different approach that can be considered in the definition of psychologically 1D models for curved pipes relies on the *theory of Cosserat* curves considered by Green and Naghdi in [21, 22] (see also [17]). If we consider the reference frame $(\hat{x}, \hat{y}, s)$ of Fig. 3 right, the basic idea of the Green and Naghdi approach is to represent the velocity field $\mathbf{u}(\hat{x}, \hat{y}, s, t)$ with respect a set of *shape functions* depending only on the coordinates in the normal section $\hat{x}, \hat{y}$:

$$\mathbf{u}(\hat{x}, \hat{y}, s, t) = \sum_{n=0}^{N} \omega_n(s, t)\boldsymbol{\varphi}(\hat{x}, \hat{y}), \tag{2.29}$$

where ω_n are the coefficients of the velocity profile. This can be considered as a generalization of the straight vessel case, where we set for the axial velocity, $u_z(x, y, z, t) = \varphi(x, y)\overline{u}(z, t)$ being $\overline{u}(z, t)$ the average velocity and $\varphi(\hat{x}, \hat{y})$ a given velocity profile. In general, when a basis functions set is selected, the unknowns are the coefficients ω_n, that can be computed by solving a suitable set of equations derived by mass and momentum conservation principles.

In principle, the accuracy of these models can be tuned by choosing a suitably large N, i.e. having a basis functions set rich enough. However, even for small values of N, mathematical difficulties of the obtained model imply high numerical costs (see [17]).

2.3.1. A curved pipe model. If we integrate any function $f(x, y, s, t)$ over the volume of pipe $V(\varepsilon)$, bounded by two normal sections at a distance ε one to the other and let $\varepsilon \to 0$, we get (see [17]):

$$\lim_{\varepsilon \to 0} \frac{1}{\varepsilon} \int_{\overline{s}-\varepsilon/2}^{\overline{s}+\varepsilon/2} \iint_{\mathcal{S}} \sqrt{g} f(x, y, \overline{s}, t) dx dy ds = \iint_{\mathcal{S}} \sqrt{g} f(x, y, \overline{s}, t) dx dy$$

where $\mathcal{S} = \mathcal{S}(\bar{s}, t)$ is the section normal to the vessel axis and $\sqrt{g}$ is the metric tensor invariant, accounting for the integration over a curved axis. In particular, for a rectlinear pipe $g = 1$, while for a curved vessel in the plane (y, s) with a constant curvature radius R_C, $\sqrt{g} = (\hat{y} + R_C)/\hat{y}$. Associated to this integral over the section $\mathcal{S}$, we introduce the following operators:

$$P_{11}(\cdot) \equiv \iint_{\mathcal{S}} \sqrt{g} \cdot d\hat{x}d\hat{y}, P_{21}(\cdot) \equiv \iint_{\mathcal{S}} \sqrt{g} \cdot \hat{x}d\hat{x}d\hat{y}, P_{22}(\cdot) \equiv \iint_{\mathcal{S}} \sqrt{g} \cdot \hat{y}d\hat{x}d\hat{y}. \tag{2.30}$$

Consider now the 3D Navier-Stokes equations written with respect to the reference frame $(\hat{x}, \hat{y}, s)$ with the velocity field represented by (2.29). In particular, we assume for the axial velocity

$$u_s = \left(1 - \frac{\hat{x}^2 + \hat{y}^2}{R^2}\right)(a(s,t) + b(s,t)\hat{x} + c(s,t)\hat{y}),$$

which is a generalization of the classical parabolic profile (first term), while for the transversal velocity components, we simply postulate a linear dependence: $u_{\hat{x}} = \dot{\eta}\hat{x}/R$, $u_{\hat{y}} = \dot{\eta}\hat{y}/R$, where $\dot{\eta}$ is the wall velocity. The unknowns of the problem are therefore the coefficients $a(s,t), b(s,t)$ and $c(s,t)$ and the vessel radius $R(s,t)$. A more convenient set of unknowns is:

$$A \equiv \pi R^2, \quad Q \equiv \frac{\pi}{2}R^2 a, \quad H \equiv \frac{\pi}{12}R^4 b, \quad G \equiv \frac{\pi}{12}R^4 c.$$

For the determination of these unknowns we need four equations that can be obtained by applying the average operator P_{11} to the continuity equation and the operators P_{11}, P_{21} and P_{22} to the axial momentum equations. The resulting psychologically 1D model reads:

$$\begin{cases} \dfrac{\partial A}{\partial t} + \dfrac{\partial Q}{\partial s} = 0 \\ \dfrac{\partial Q}{\partial t} + \dfrac{1}{R_C}\dfrac{\partial G}{\partial t} + \dfrac{4}{3}\dfrac{\partial}{\partial s}\dfrac{Q^2}{A} + 6\pi\dfrac{\partial s}{\partial}\dfrac{H^2}{A^2} + \dfrac{\beta\sqrt{A}}{2\rho A_0}\dfrac{\partial A}{\partial s} + 8\pi\nu\dfrac{Q}{A} + \dfrac{24\pi\nu}{R_C}\dfrac{G}{A} = 0 \\ \dfrac{\partial H}{\partial t} + 2\dfrac{\partial}{\partial s}\dfrac{HQ}{A} + \dfrac{1}{2}\dfrac{H}{A}\dfrac{\partial Q}{\partial s} + 24\pi\nu\dfrac{H}{A} = 0 \\ \dfrac{\partial G}{\partial t} + \dfrac{1}{6\pi R_C}\dfrac{\partial QA}{\partial t} + 2\dfrac{\partial}{\partial s}\dfrac{GQ}{A} + \dfrac{G}{2A}\dfrac{\partial Q}{\partial s} + \dfrac{\hat{\beta}}{A^{3/2}}\dfrac{\partial A}{\partial s} + 24\pi\nu\dfrac{G}{A} + \hat{\nu}Q = 0 \end{cases} \tag{2.31}$$

where $\hat{\beta} := \beta/(8\pi\rho A_0 R_C)$, $\hat{\nu} := 3\nu/R_C$.

More complex model can be devised for instance by assuming a different profile for the transversal velocity components (see [17]).

In Fig. 4 we illustrate the solution of (2.31) at different time steps for a curved planar pipe with $R_C = 5\,\text{cm}$. G is non null because of the curvature of the pipe (taken from [17]), while H is null since the pipe is planar.

In Fig. 5 the solution for a pipe with $R_C = 1\,\text{cm}$ is shown in order to outline the asymmetry on the axial velocity profile induced by the curvature (taken from [17]).

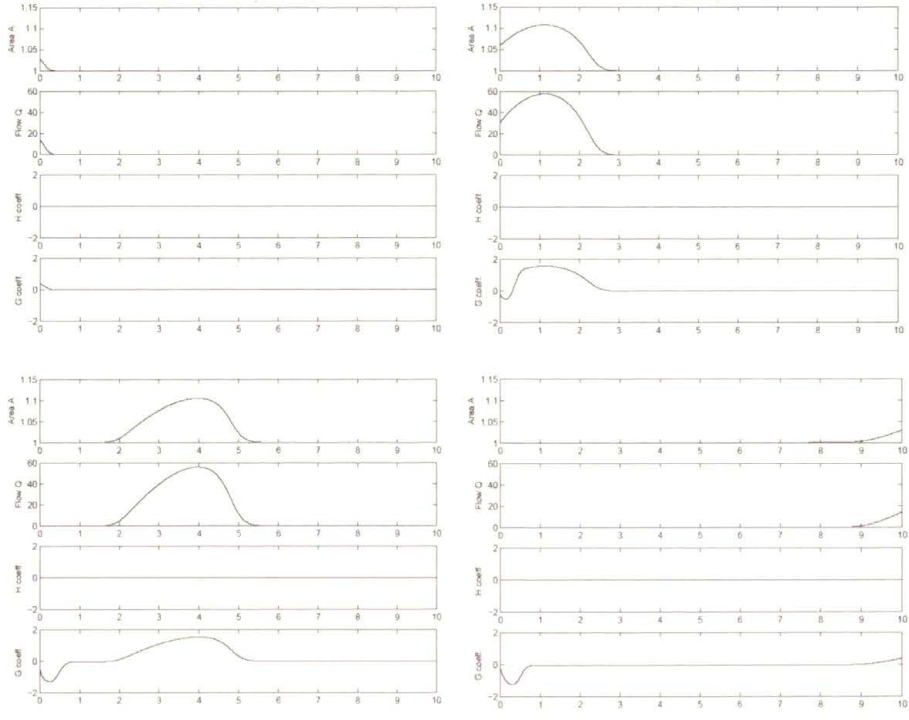

FIGURE 4. Solution (A, Q, H, G respectively) at $t = 0.0005\,\text{s}$ (top, left), $t = 0.005\,\text{s}$ (top, right), $t = 0.010\,\text{s}$ (bottom, left), $t = 0.025\,\text{s}$ (bottom, right) for the model (2.31), with $R_C = 5\,\text{cm}$ (the pipe length is 5 cm). A wave comes into the pipe at the inlet. H is null due to the symmetry of the problem (curved pipe in the (x, s) plane). G is $\neq 0$ for the presence of the curvature. Pictures taken from [17].

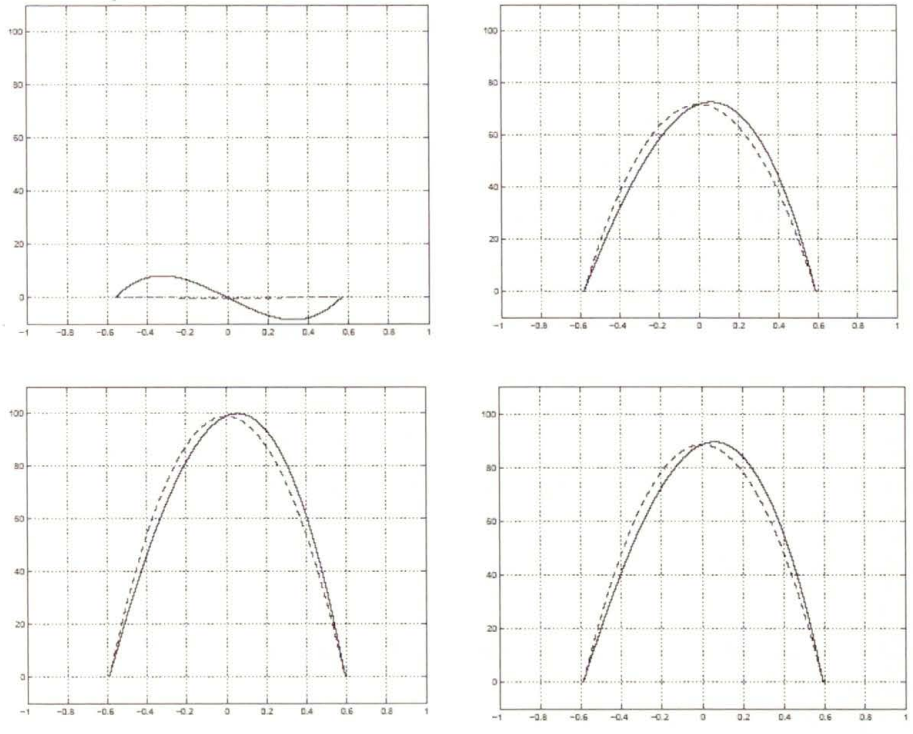

FIGURE 5. Solution in a curved pipe with $R_C = 1\,\text{cm}$ at $t = 0.005\,\text{s}$ for different values of the curvilinear abscissa s. Representation of the axial velocity profiles along $\hat{x}$ (continuous line) and $\hat{y}$ (dotted line). The asymmetry of the profile induced by the curvature is evident. Pictures taken from [17].

2.4. Simple-minded Models of Blood Solutes Dynamics

In haemodynamics simulations it is sometimes of interest not only the blood dynamics, but also the dynamics of solutes (oxygen, lipids, etc.) which are convected by the blood to the tissues and peripheral organs (see e.g. [51, 52, 69]). In the perspective of setting up a multiscale model for the circulation, we therefore need some simplified models also for the blood solutes. Suppose that the solute concentration $\gamma(\mathbf{x}, t)$ fulfills a (linear) advection-diffusion equation in the form

$$\frac{\partial \gamma}{\partial t} - \mu \triangle \gamma + \mathbf{u} \cdot \nabla \gamma = 0$$

in the domain Ω_t ($\mathbf{u}$ is the blood velocity), together with a suitable initial condition $\gamma(\mathbf{x}, 0) = \gamma_0(\mathbf{x})$. A Dirichlet condition $\gamma = \gamma_{\text{ext}}$ can be given on

the vascular wall [12] or more realistically a Robin condition $\mu\nabla\gamma\cdot\mathbf{n} = \alpha(\gamma_{\text{ext}}-\gamma)$ ($\mathbf{n}$ unit outward normal vector, [67]). By proceeding in a way similar to the one adopted for the Navier-Stokes equations, it is possible to deduce a "simple-minded" model for the blood solute dynamics (see [12, 67]). More precisely, let $\Gamma = A\gamma$ be the *linear concentration*. It is possible to deduce for Γ in a cylindrical straight vessel with $z \in (0,l)$ the 1D equation:

$$\frac{\partial\Gamma}{\partial t} + \frac{\partial}{\partial z}\left(\omega\frac{\Gamma Q}{A}\right) + K_c\frac{\Gamma}{A} = f(\gamma_{\text{ext}}) \tag{2.32}$$

to be completed with suitable boundary condition. Here, K_c is a coefficient depending on the viscosity μ and the concentration profile over the transversal section and ω depends on the axial blood velocity. Equation (2.32) can be therefore coupled to (2.11) for a model of the blood and solutes dynamics. For instance, in Fig. 6 (taken from [67]) the concentration at a given instant of the simulation is shown in a bifurcation in the neighborhood of the bifurcation tip.

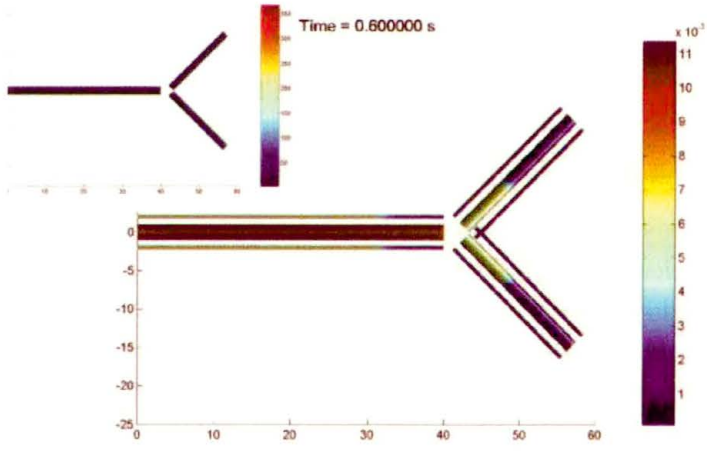

FIGURE 6. Concentration of a blood solute computed with the 1D model (2.32) coupled with 1D blood flow model (2.11) (small picture on the left) in a bifurcation geometry. Picture taken from [67]

3. Lumped Parameters Models for the Circulation

Many biological systems feature complex mechanisms given by the interaction of elementary components. A possible and effective description of such systems is based on the identification of these elementary components, often called *compartments* (see e.g. [9]) and their mutual interaction. In the case of cardiovascular modeling, we could say that *a compartment is a part of the system which is reasonable to consider as a whole, according to the needed accuracy in the description of circulation. The behavior of the blood in a compartment is described in terms of quantities (typically the flow rate and pressure) "averaged" (in space) over the whole compartment.* The mathematical description of this system can be therefore provided by:

1. the description of each compartment;

2. the description of the interactions among the compartments.

The number of the compartments involved depends on the level of accuracy requested to the model. For instance, if one wants to investigate heart failures with the purpose of increasing the cardiac function without a significant (and dangerous) increment of the systolic pressure, a two-compartments description of the cardiovascular system can be enough, featuring the left ventricle and the systemic circulation respectively (see [38], Chap. 13). The *Windkessel* and *Westkessel* models are instances of two-compartments model (the heart and the vascular system), the latter featuring a more precise description of the vascular compartment. More complex examples can be found in [27], Chap. 5, and [29], Chap. 14, where an accurate sensitivity analysis of the parameters of a four-compartments description of the cardiovascular system is carried out. Other references are [30] and [66]. A recent derivation of lumped parameter models based on the Laplace transformation can be found in [41].

Lumped parameters models that we are going to introduce in view of multiscale modeling are, in fact, compartments models which can be described by following the two steps mentioned above. In particular we will firstly introduce lumped parameters models (Sec. 3.1 and 3.2) for a simple compliant cylindrical vessel and for the heart. Then in Sect. 3.3, we will consider the assembly of models for the whole circulation.

3.1. Lumped Parameter Models for a Cylindrical Compliant Vessel

Let us consider again the simple cylindrical artery Ω illustrated in Fig. 1. Starting from equations (2.11), we observe that

$$\frac{\partial A}{\partial t} = 2\pi R \frac{d\eta}{dt} \approx 2\pi R_0 \frac{\partial \eta}{\partial t},$$

and we will assume

$$\frac{\partial A}{\partial t} = \frac{3\pi R_0^3}{2Eh} \frac{\partial P}{\partial t}.$$

In the sequel, we will set

$$k_1 := \frac{3\pi R_0^3}{2Eh}.$$

In order to provide a lumped description of the behavior of the blood in the whole district Ω we need to perform a further averaging of (2.11) over the axial coordinate. To this aim, it is useful to introduce the following notation. We define as *the (volumetric) mean flow rate over the whole district* the quantity

$$\hat{Q} = \frac{1}{l} \int_{\mathcal{V}} u_z d\upsilon = \frac{1}{l} \int_0^l \int_{\mathcal{A}(z)} u_z d\sigma dz = \frac{1}{l} \int_0^l Q dz. \tag{3.1}$$

Similarly, we define the *mean pressure over the whole compartment* as

$$\hat{p} = \frac{1}{l} \int_0^l P dz. \tag{3.2}$$

Integrating over the axial coordinate, and assuming that (see [3]):

1. the contribution of the convective terms may be neglected,
2. the variation of A with respect to z is small compared to that of P and Q,

we obtain the equations:

$$k_1 l \frac{d\hat{p}}{dt} + Q_2 - Q_1 = 0 \tag{3.3}$$

and

$$\frac{\rho l}{A_0} \frac{d\hat{Q}}{dt} + \frac{\rho K_R l}{A_0^2} \hat{Q} + P_2 - P_1 = 0 \tag{3.4}$$

where

$$\begin{aligned} Q_1(t) &:= Q(t,0), \qquad & P_1(t) &:= P(t,0), \\ Q_2(t) &:= Q(t,l), \qquad & P_2(t) &:= P(t,l). \end{aligned} \tag{3.5}$$

These equations represent a lumped parameters description of the blood flow in the compliant cylindrical vessel Ω, and involve the mean values of the flow rate and the pressure over the domain, as well as the upstream and downstream flow rate and pressure values. The coefficients in equations (3.3), (3.4) have been obtained from the integration process. They are in fact the lumped parameters which summarize the basic geometrical and physical features of the dynamic system formed by the blood flow and the vessel wall. Let us try to summarize their meaning.

R In (3.4) we set $R := (\rho K_R l)/(A_0^2)$. If we assume a parabolic velocity we have

$$R = \frac{8\pi\rho\nu l}{\pi^2 R_0^4} = \frac{8\mu l}{\pi R_0^4},$$

where R represents the *resistance* induced to the flow by the blood viscosity. Different expressions for R can be obviously obtained for different velocity profiles or if a non Newtonian rheology is introduced into the model (see e.g. [3, 53, 64]).

L In (3.4) we set $L := (\rho l)/(A_0) = (\rho l)/(\pi R_0^2)$. L represents the inertial term in the momentum conservation law and will be called the *inductance* of the flow.

C In (3.3) we set $C := k_1 l = (3\pi R_0^3 l)/(2Eh)$. C represents the coefficient of the mass storage term in the mass conservation law, due to the *compliance* of the vessel.

With this notation, equations (3.3), (3.4) becomes

$$\begin{cases} C\dfrac{d\hat{p}}{dt} + Q_2 - Q_1 = 0 \\ L\dfrac{d\hat{Q}}{dt} + R\hat{Q} + P_2 - P_1 = 0. \end{cases} \tag{3.6}$$

Now, assume that some upstream and downstream data are available. For instance, suppose that Q_1 *and* P_2 *are given.* Then, (3.6) represents a system of two equations for four unknowns, $\hat{Q}$, $\hat{p}$, P_1 and Q_2. In order to close mathematically the problem we need some further assumptions. In particular, the dynamics of the system is represented by $\hat{p}$ and $\hat{Q}$, i.e. by the unknowns that are under time derivative (the *state variables*), so it is reasonable to

approximate the unknowns on the upstream and downstream sections with the state variables, that is

$$\hat{p} \approx P_1, \quad \hat{Q} \approx Q_2.$$

With these additional assumptions, which are reasonable for a short cylindrical pipe, the lumped parameters model becomes:

$$\begin{cases} C\dfrac{dP_1}{dt} + Q_2 = Q_1 \\ L\dfrac{dQ_2}{dt} + RQ_2 - P_1 = P_2. \end{cases} \tag{3.7}$$

where the upstream and downstream prescribed data have been plugged into the right hand side. This system can be illustrated by the electric $\mathcal{L}$-network shown in Fig. 7 (left). The compliance has been gathered on section Γ_1, where the flow rate is prescribed, and the inertial effects have been allocated on Γ_2, where the mean pressure is provided.

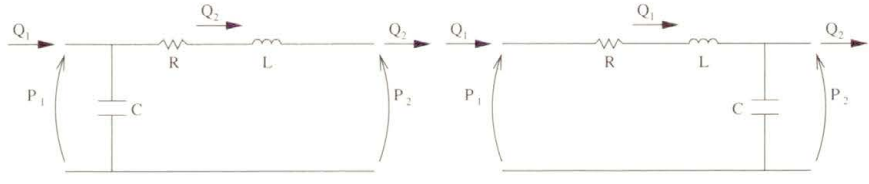

FIGURE 7. Lumped $\mathcal{L}$-network (left) and $\mathcal{L}$-inverted network (right) equivalent to a short pipe

In the electric network analogy, the blood flow rate is assimilated to the current, while the blood pressure corresponds to the voltage (see Tab. 1).

In a similar way, if the pressure P_1 and the flow rate Q_2 are prescribed, we still approximate the unknown quantities on the upstream and downstream

TABLE 1. Correspondence table of the analogy between electric and hydraulic networks.

HYDRAULIC	ELECTRIC
Pressure	Voltage
Flow rate	Current
Blood viscosity	Resistance R
Blood inertia	Inductance L
Wall compliance	Capacitance C

sections with the state variables, i.e. $\hat{p} \approx P_2, \quad \hat{Q} \approx Q_1$, yielding the system whose electric analog, called $\mathcal{L}$-inverted network, is given in Fig. 7, right.

The case when the mean pressures P_1 and P_2 are prescribed, can be modelled by a cascade connection of $\mathcal{L}$ and $\mathcal{L}$-inverted lumped representations, yielding a $\mathcal{T}$-network (Fig. 8). Similarly, if both the flow rates Q_1 and Q_2 are prescribed, the the vessel Ω is described by the electric π-network, obtained as a cascade connection of a $\mathcal{L}$-network and a $\mathcal{L}$-inverted network (Fig. 9).

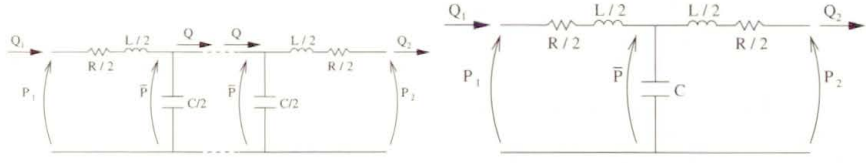

FIGURE 8. Cascade connection of a $\mathcal{L}$-inverted and a $\mathcal{L}$-network (left), lumped $\mathcal{T}$-network (right).

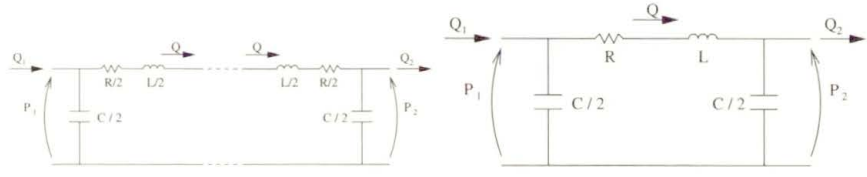

FIGURE 9. Cascade connection of a $\mathcal{L}$-network and a $\mathcal{L}$-inverted one (left), lumped π-network (right).

Let us observe that the four different circuits arise from four different possible assumptions about the kind of data prescribed on the upstream and downstream sections. With a little abuse of notation we could call them "boundary data"[1]. The four different lumped models can be considered therefore as the lumped parameters simplification of four different "boundary" values problems.

Finally observe that some of the simplifying assumptions introduced can be removed (or reduced) by modifying the network: for more details, see [3].

[1] Actually, in the simplification leading to lumped parameters models the dependence on the space variables has been lost in the averages, so there is no "boundary" of the domain.

3.2. Lumped Parameters Models for the Heart

The heart is a special "compartment" of the vascular system that need a specific representation in the lumped parameters framework. The structure of the heart and its relationship with its functionality are not completely understood and recent investigations show that the ventricular myocardium can be unwrapped by blunt dissection into *a single continuous muscle band* (see [59]). This could modify the accurate mathematical modeling as well as medical investigations and surgical interventions on the heart. For the purpose of these notes, however, we simply refer to a classical description of the heart, which is subdivided into two parts, called to the right and the left heart, respectively, separated by the *septum*. The right heart supplies the pulmonary circulation, while the left pumps the blood into the systemic tree. Each side consists of two chambers, the atrium and the ventricle, seprated by the atrioventricular valves (the *tricuspid* valve in the right side, the *mitral* valve in the left one). Their role is to receive fluid at low pressure and transfer it to a higher pressure region. In other words, each side acts as a *pump* (see [27]). Each ventricle can be described *as a vessel where the most significant feature is the compliance* and *the compliance changes with time* (see [10, 27, 29, 55]).

The starting point for a possible mathematical model is the relation that links pressure and radius of an elastic spherical ball filled with fluid. Here and in the following we take $P_{\text{ext}} = 0$. We have

$$\pi R^2 P = 2\pi E h_0 R \frac{R - R_0}{R_0},$$

where R_0 is the reference sphere radius, which is the one reached when $P = 0$, h_0 a reference thickness of the ball surface and E the Young modulus. The contraction of the cardiac muscle may be taken into account by an increase of E (stiffening) and by a shortening of the muscle length (that is a reduction of R_0). It is more convenient to express this relation as a function of the volume V, instead of the radius. By recalling that $V = 4\pi R^3/3$, a linearisation procedure leads to

$$P = \frac{E(t)h_0}{2\pi R_0^3(t)} \left(V - V_0(t)\right),$$

where we have indicated the coefficients that change in time because of the action of the muscle. This simplified model does indeed describe the major

characteristic of the ventricle. If we indicate

$$C(t) = \frac{2\pi R_0^3(t)}{E(t)h_0},$$

we may re-write the relation in the more compact form

$$V(t) = C(t)P(t) + V_0(t).$$

By deriving with respect to time we obtain

$$\frac{dV}{dt} = Q = \frac{dC}{dt}P + C\frac{dP}{dt} + M_Q(t) \tag{3.8}$$

where Q represents the (incoming) flow rate and $M_Q = dV_0/dt$ is the action exerted by the contraction of the cardiac muscle.

A lumped representation (electric analog) of each ventricle[2)] is given in Fig. 10, where R accounts for an additional viscous resistance inside the ventricle, whose relevance has been recently pointed out by [58] and M_Q is represented by a generator of current.

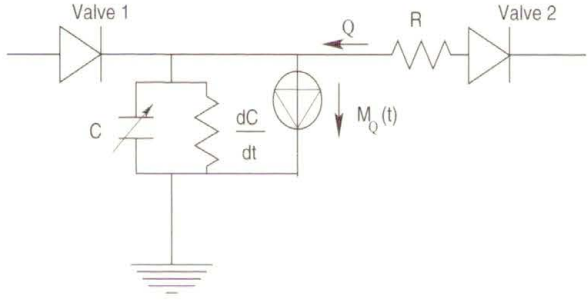

FIGURE 10. Network for the lumped parameters modeling of a ventricle.

In Fig. 10 the presence of heart valves has been taken into account by *diodes* which allow the current flow in one direction only[3)]. Observe that the presence of the valves *introduces a nonlinear relation* in the lumped parameters model.

[2)] A mechanical representation of the heart working based on the classical Hill's model for the muscle can be found in [30] and [66]. See also [2]

[3)] The same representation can be used also for the valves in the venous system, whenever needed.

3.3. Lumped Parameters Models for the Circulatory System

The compartments previously described are the elementary bricks for building models for the whole system. As previously pointed out, the number of compartments depends on the accuracy requested to the model and, definitely, on the number of vessels that it is worthwhile to represent separately as single units.

The connection among the compartments is driven by *flux and momentum conservation* at the interfaces. As a direct consequence of the electric analogy the quantities that are matched are Q and the pressure P. There is a difference in this respect to the coupling of 1D models (see Sect. 2.2), where the total pressure is considered. This choice is indeed consistent with the hypothesis of negligible convective terms.

In the electric analog, these relations correspond to the application of the classical *Kirchhoff laws* for the nodes (conservation of current) and the nets (conservation of the voltage). An sketch of the possible connection of different compartments is given in Fig. 11.

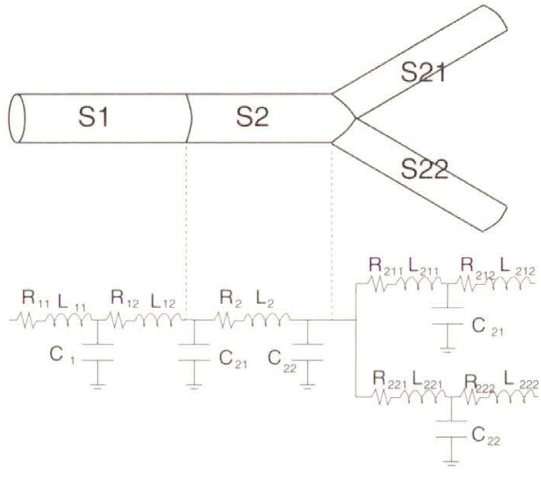

FIGURE 11. Lumped parameters model for a branched vessel as a cascade of T and π networks.

A detailed electric analog for the circulation is provided in [64] and in [40], where hundreds of elementary compartments are accounted for.

From the mathematical viewpoint, a general representation of lumped parameters models is a Differential-Algebraic-Equations (DAE) system in

the form

$$\begin{cases} \dfrac{d\mathbf{y}}{dt} = B(\mathbf{y}, \mathbf{z}, t) \quad t \in (0, T] \\ G(\mathbf{y}, \mathbf{z}) = 0 \end{cases} \tag{3.9}$$

together with the *initial condition vector* $\mathbf{y}|_{t=t_0} = \mathbf{y}_0$. Here, $\mathbf{y}$ is the vector the state variables (associated to capacitors and inductors), $\mathbf{z}$ are other variables of the network and G the algebraic equations that derive from the Kirchhoff laws. If we suppose that the Jacobian matrix $J := \partial G/\partial \mathbf{z}$ is non singular[4)], by the implicit function theorem we can express $\mathbf{z}$ as function of $\mathbf{y}$ and resort to the reduced Cauchy problem

$$\begin{aligned} &\frac{d\mathbf{y}}{dt} = \mathbf{\Phi}(\mathbf{y}, t) = A(\mathbf{y}, t)\mathbf{y} + \mathbf{r}(t) \quad t \in (0, T], \\ &\mathbf{y} = \mathbf{y}_0, \quad \text{at } t = t_0. \end{aligned} \tag{3.10}$$

The time dependence of matrix A is due to the heart action and is related to the variable ventricles compliances, while the dependence of A on $\mathbf{y}$ is due to the presence of diodes (non linear term). The forcing term $\mathbf{r}$ depends on t through the function $M_Q(t)$.

From classical results of calculus, it is possible to prove that (a) if $\mathbf{\Phi}(\mathbf{y}, t)$ is continuosly differentiable there exists a time interval $[0, T^*]$ in which the solution of the problem exists and is unique; (b) if, moreover, the derivatives $\partial \mathbf{\Phi}_i/\partial y_j$ are bounded in all the time interval $[0, T]$, then the solution of the Cauchy problem exists and is unique in $[0, T]$.

In the sequel, we will suppose that the previous hypotheses are verified.

From the numerical point of view, the nonlinear ordinary differential system (3.10) can be solved by means of classical methods. For this reason we do not dwell here with the numerical solving of lumped parameter models and refer the interested reader to e.g. [47].

4. Basic Numerical Issues for Multiscale Modeling

Our goal is now to investigate specific problems arising from the mathematical and numerical coupling of different models for blood flow, ranging from the Navier-Stokes equations down to lumped parameters models. In particular, we will have to manage the interfaces between models featuring a different level of detail. It is to be expected that the more accurate (pointwise) model would need on the interfaces more data than the mean models

[4)] In this case, the DAE system is said to be *of index 1*.

could give, being by far less accurate. The data referred to the simple-minded submodel are indeed a spatial average of the pointwise quantities which are, on the other side, considered by the accurate local submodel and that would be needed on the interfaces in order to make it well posed the Navier-Stokes boundary problem. We have, therefore, the problem of giving a well posed formulation of the local subproblem, filling up the defective data set provided by the reduced submodels. The main concern of multiscale modeling is to carry out this completion minimizing, as far as possible, the perturbations on the numerical solution. For example, if the flow rate (*mean value*) is known on the upstream section of a vascular district, there are many velocity profiles (*pointwise values*) on that section that can be associated to such mean data and, therefore, can be prescribed to the Navier-Stokes problem. However, the choice of a specific profile will strongly influence (or perturb) the numerical solution in a non-controlled way. The present Section illustrates some techniques for avoiding the prescription of a velocity profile and, in general, for reducing perturbations on the numerical solution when solving 3D problems with average (defective) boundary data.

4.1. Defective Boundary Data Problems

For the sake of clarity, let us provide a general statement of defective boundary data problems. Let Ω be a bounded domain of $\mathbb{R}^d$, $d = 2$ or 3, whose boundary $\partial\Omega$ is decomposed into the union of Γ_{wall} and several disjoint sections $\Gamma_0, \Gamma_1, \ldots, \Gamma_n$, $n \geq 1$ (see Fig. 12).

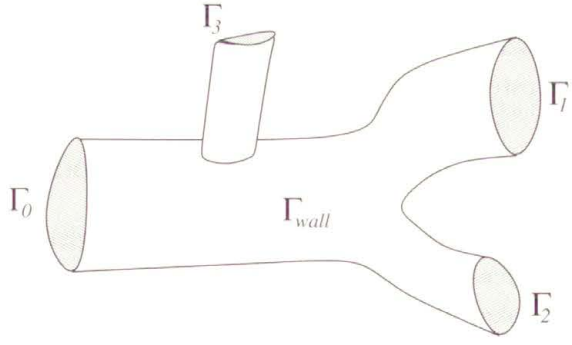

FIGURE 12. The partition of the boundary of the domain Ω.

For the sake of simplicity, we suppose that the domain is rigid, so that we are interested in solving the Navier-Stokes equations in Ω:

$$\begin{cases} \dfrac{\partial}{\partial t}\mathbf{u} + \mathbf{u}\cdot\boldsymbol{\nabla}\mathbf{u} + \boldsymbol{\nabla}p - \nu\triangle\mathbf{u} &= \mathbf{f}, & t>0 \\ \operatorname{div}(\mathbf{u}) &= 0, & t>0 \\ \mathbf{u} &= \mathbf{u}_0, & t=0, \\ \mathbf{u} &= 0 & \mathbf{x}\in\Gamma_{\text{wall}}. \end{cases} \tag{4.1}$$

Two different kinds of boundary conditions are of some interest in the multiscale coupling and will be considered on the sections Γ_i, $i=0,\ldots,n$.

The first condition refers to the *mean pressure problem*, which requires that

$$\frac{1}{\operatorname{meas}(\Gamma_i)}\int_{\Gamma_i} p\,ds = P_i(t), \quad i=0,\ldots,n. \tag{4.2}$$

The second condition we address is the *flow rate problem*

$$\int_{\Gamma_i} \mathbf{u}\cdot\mathbf{n}\,ds = Q_i(t), \text{ for } i=0,\ldots,n. \tag{4.3}$$

Observe that, due to the fluid incompressibility and the rigidity of the wall, a compatibility relation must exist among the fluxes Q_i, namely:

$$Q_0 + Q_1 + \ldots + Q_n = 0. \tag{4.4}$$

The initial-boundary value problem (4.1) with either (4.2) or (4.3) is not well-posed from a mathematical point of view due to the average (non-pointwise) nature of the boundary data on the artificial boundaries (see [61]). A possible way for completing the lackness of data is the one proposed in [26]. Following this approach, a particular *weak or variational formulation of the boundary problem* is devised which allows to fulfill conditions (4.2) (resp. (4.3)) at some extent, giving rise to a well-posed problem. In fact, this formulation forces in an implicit way some natural (Neumann-like) boundary conditions which selects one particular solution among all the possible ones of the original differential problem. The completition of the defective boundary data set is essentially an implicit by-product of the choice of the suitable variational formulation, which is based on a natural set of boundary conditions, less perturbative than essential (Dirichlet) ones.

This approach is really effective for the numerical solution of the mean pressure drop problem (see [61]). In solving the flow rate problem, it is not

straightforward for what concerns the selection of an appropriate finite dimensional space for the space discretization. Here, we will address therefore a reformulation of the flow rate problem proposed in [16], more suitable for the numerical purposes.

4.1.1. A Lagrange multiplier approach for flow rate boundary conditions. Consider the initial-boundary values problem given by (4.1) and the net flux conditions (4.3). We assume that the compatibility condition (4.4) is fulfilled.

Rather than (defective) boundary conditions, (4.3) can be regarded as a set of *constraints* for the solution of the problem at hand. Starting from this viewpoint, a possible way for forcing such constraints resorts to the Lagrange multiplier approach. According to this strategy, the equations to be solved are *penalized* by the presence of the constraint, weighted by suitable (unknown) coefficients, the Lagrange multipliers[5]. The original problem is therefore reformulated in an *augmented* fashion, due to the presence of the multipliers (see e.g. [23]).

In the present case, this approach leads to the following variational problem: look for $\mathbf{u} \in V$, $p \in M$ and $\lambda_1, \ldots, \lambda_n \in \mathbb{R}$ such that, for all $\mathbf{v} \in V$ and $q \in M$,

$$\begin{cases} \left(\dfrac{\partial}{\partial t}\mathbf{u} + \mathbf{u} \cdot \boldsymbol{\nabla}\mathbf{u}, \mathbf{v}\right) + \nu(\boldsymbol{\nabla}\mathbf{u}, \boldsymbol{\nabla}\mathbf{v}) + \displaystyle\sum_{i=1}^{n} \lambda_i \int_{\Gamma_i} \mathbf{v} \cdot \mathbf{n} - (p, \operatorname{div}(\mathbf{v})) = \langle \mathbf{f}, \mathbf{v} \rangle, \\ (q, \operatorname{div}(\mathbf{u})) = 0, \\ \langle \phi_i, \mathbf{u} \rangle = Q_i, \qquad i = 0, \ldots, n, \end{cases} \tag{4.5}$$

for all $t > 0$, with $\mathbf{u} = \mathbf{u}_0$ for $t = 0$.

The mathematical analysis of this probem (its equivalence to the mean flux problem stated above and its well-posedness) can be found in [16] and [62].

In order to discretize equation (4.5), we introduce a Galerkin approximation based on the finite dimensional spaces $V_h \subset V$ and $M_h \subset M$, which we assume to satisfy the well-known LBB condition (see e.g [48], Chap. 9.):

$$\forall q_h \in M_h \quad \exists \mathbf{v}_h \in V_h,\ \mathbf{v}_h \neq 0 : \quad (q_h, \operatorname{div}(\mathbf{v})_h) \geq \beta_h |q_h|_{L^2} |\mathbf{v}_h|_{H^1}. \tag{4.6}$$

[5] We remind that in the same perspective, the pressure of the incompressible Navier-Stokes equations can be regarded as the Lagrange multiplier of the incompressibility constraint—see e.g. [48].

Let $(\mathbf{u}_h, p_h, \lambda_{1h}, \ldots, \lambda_{nh})$ be the solution of the discrete problem. We denote by $(u_i)_{i=1\ldots dN}$ (resp. $(p_i)_{i=1\ldots M}$) the components of $\mathbf{u}_h$ (resp. p_h) with respect to a basis $\{\mathbf{v}_i\}$ of V_h (resp. $\{q_i\}$ of M_h). Finally, we introduce the vectors $U = (u_1, \ldots, u_{dN}) \in \mathbb{R}^{dN}$, $P = (p_1, .., p_M) \in \mathbb{R}^M$ and $\Lambda = (\lambda_{1h}, \ldots, \lambda_{nh}) \in \mathbb{R}^n$. Then the discrete counterpart of (4.5) gives rise to the following algebraic system of equations

$$\left\{ \begin{array}{rcl} AU + D^T P + \Phi^T \Lambda &=& F, \\ DU &=& 0, \\ \Phi U &=& Q, \end{array} \right. \tag{4.7}$$

where $A \in \mathbb{R}^{dN \times dN}$ is the stiffness matrix, $D \in \mathbb{R}^{M \times dN}$ is the matrix associated to the divergence operator and Φ is the $n \times dN$ matrix whose lines are given by the vectors $\phi_i = (\int_{\Gamma_i} \mathbf{v}_1 \cdot \mathbf{n}\, ds, \ldots, \int_{\Gamma_i} \mathbf{v}_{dN} \cdot \mathbf{n}\, ds)$, $i = 1, \ldots, n$.

It is possible to prove that this system is non singular, [16]. However, this system is not a classical Navier-Stokes problem, so its numerical solution should require the set up of an "ad hoc" solver. On the other hand, there is no numerical convenience in setting up a solver computing simultaneously U, P and Λ, since the matrix associated to system (4.7) is supposed to be very ill conditioned in real applications. Therefore, as for the standard Navier-Stokes problem (see [48]), it is worthwhile to resort to splitting methods which reduce the problem to a series of smaller and easier to solve steps. This can be done in different ways (see [62]). Here we illustrate a strategy that has the advantage of separating the fluid (velocity and pressure) from the multipliers computation. In this way, if a Navier-Stokes solver is available (for instance a commercial package), it can be actually adopted for solving the augmented problem.

We rewrite (4.7) in the form

$$\begin{bmatrix} S & \tilde{\Phi}^T \\ \tilde{\Phi} & 0 \end{bmatrix} \begin{bmatrix} X \\ \Lambda \end{bmatrix} = \begin{bmatrix} G \\ Q \end{bmatrix} \tag{4.8}$$

where $\tilde{\Phi} = [\Phi, 0] \in \mathbb{R}^{n \times (dN+M)}$, $X = [U, P]^T$, $G = [F, 0]^T$. The matrix S corresponds to the discretization of the Navier-Stokes problem with Neumann conditions on the boundaries where the net fluxes are prescribed. If the two discrete spaces V_h and M_h satisfy the LBB condition (4.6), S is non singular (see, e.g. [8, 48]). We can then eliminate the unknown X from (4.8), obtaining a system for the Lagrange multiplier:

$$\tilde{\Phi} S^{-1} \tilde{\Phi}^T \Lambda = \tilde{\Phi} S^{-1} G - Q. \tag{4.9}$$

This system can be solved by an appropriate iterative method. For instance, if we denote $R := \tilde{\Phi} S^{-1} \tilde{\Phi}^T$ and $\mathbf{b} := \tilde{\Phi} S^{-1} G - Q$, we could resort to the classical preconditioned GMRes scheme[6] (see e.g. [54]). In particular, this requires to solve a Navier-Stokes problem at each iteration and this can be carried out by means of a standard solver. This could seem quite expensive. However, the matrix R is usually small, being its dimension equal to the number of artificial boundaries, so the number of iterations required will be accordingly small. Moreover, the computational efficiency can be improved by finding good preconditioners of R. Other approaches rely on finding suitable approximations for system (4.7) cheaper to solve (see e.g. [63]).

4.1.2. Numerical results. In order to assess the proposed methodologies, we consider a case where the analytical solution of the Navier-Stokes equations is known. More precisely, we consider the *Womersley* solution, which describes the transient flow in a cylindrical pipe associated to a time-periodic pressure gradient (see e.g. [38]). As such, it is a transient counterpart of the well known Poiseuille solution.

We have considered a straight cylinder, imposing homogeneous Neumann boundary conditions at the inflow, while at the outflow we prescribe the flow rate associated to the Womersley solution. The results are shown in Fig. 13. Here, the computed velocity field at two different times is illustrated, together with the corresponding exact axial velocity profile. The solution obtained agrees very well with the analytical one. A single condition on the flow rate at the outflow, imposed through a Lagrange multiplier, is sufficient to recover the Womersley flow. It is worthwhile outlining that *the Womersley profile is an outcome of the computation, it has not been forced anyway.* Other analytical tests can be found in [62].

In Fig. 14 we report the solution of the net flux problem obtained by solving a steady flow rate problem with the Lagrange multiplier approach in a real geometry of the total cavopulmonary connection. The solution has been obtained with a commercial solver (Fluent). Again, we point out that the velocity profiles are not prescribed but they are an outcome of the numerical simulation.

[6] In the case of a Stokes problem, R is symmetric and positive definite, so the Conjugate Gradient method can be adopted.

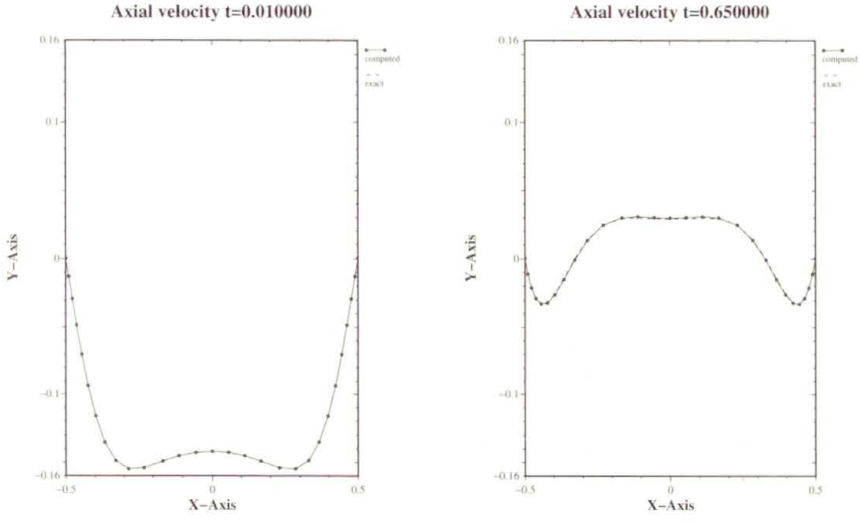

FIGURE 13. 3D numerical solutions obtained at two different instants imposing a periodic flux. The continuous line is the numerical solution, the dotted line is the analytical one.

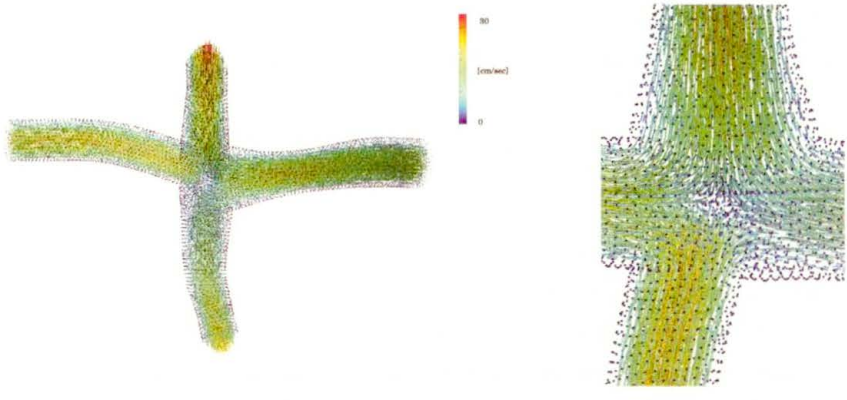

FIGURE 14. Cavo-pulmonary connection: velocity field computed with the Lagrangian multiplier approach. Simulations carried out with a commercial solver (Fluent).

5. Multiscale Models

Having developed techniques for managing local 3D problems with mean boundary data in a numerically sound way, we are now in position of describing complete geometrical multiscale models, both from a mathematical and numerical viewpoints. We will start considering a 3D and a 0D model, discussing its well posedness and numerical methods for the coupling. Then, we will address numerical methods for 3D-1D coupling (Sect. 5.2). We will finally consider the coupling of 1D and 0D models.

Numerical results of medical interest are presented in Sect. 6.

5.1. Coupling 3D and 0D Models

We wish to represent the whole circulatory system by an electric circuit except on a specific region Ω, where blood flow is modelled by the Navier-Stokes equations, as illustrated in in Fig. 15. Here, the compliance of the local vascular district is neglected for the sake of simplicity, hence Ω is constant in time. Let us assume that the network faces the district Ω by capacitors C_i ($i = 1, \ldots, \overline{n}$) as shown in the picture. In particular, we put in evidence the representation in terms of a network of the vascular regions in the immediate neighborhood of the 3D model. In [50] we have extensively investigated this problem. In particular these parts of the lumped network have been called the *bridging regions*. In this picture, we have three bridging regions corresponding to the three inflow/outflow of Ω. We are essentially coupling a lumped representation of the circulation with the mean pressure problem for the Navier-Stokes equations. The boundary mean pressures are not given, but are state variables of the lumped model to be computed. The heterogeneous multiscale problem is therefore given by coupling subproblems that can be proved to be separately well posed. It is reasonable to expect that the global multiscale model is well posed. This well posedness has been proved in [50] starting from classical fixed point techniques.

The role of the interface conditions in the splitting procedure is naturally driven by the specific topology of the network at the interfaces. In the case of Fig. 15, the interface flow rates are not state variables of the lumped system, and, therefore, they are well suited to play the role of a forcing term for the ordinary differential system. However, depending on the choice of the bridging regions, the matching between the network and the Navier Stokes system could be pursued, for instance, by interchanging the role of flux and pressure at the interfaces.

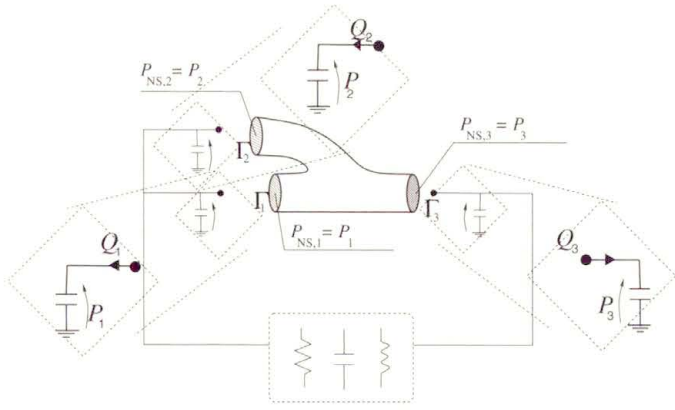

FIGURE 15. Scheme of coupling between the whole system and a local district. The lumped representation of the three bridging regions at the interfaces with the Navier-Stokes model is highlighted in the dashed circles.

In this case we should suppose that the flow rates are provided to the Navier-Stokes system by the network, which in turn receives pressure data. For instance, in the network configuration of Fig. 16, the interface pressure is not a state variable of the lumped system, so it is a good candidate for being a forcing term of the ordinary differential system, provided by the Navier-Stokes solution. On the other hand, the interface flow rates, which in the electric analogy correspond to the current at the interfaces and are state variables for the system, become boundary data for the Navier-Stokes problem. In this case, we formulate a net flux problem for the Navier-Stokes model, to be faced according to the Lagrange multiplier approach.

For the numerical treatment of these coupled models, it is natural to resort to an iterative approach based on the splitting of the whole problem into its basic components, the ODE system from one hand and the Navier-Stokes equations from the other one.

For the sake of clarity, suppose to deal with the coupled problem represented in Fig. 16. A compact representation of a possible numerical scheme is given in Fig. 17 (left). In this scheme, an explicit time advancing method is used for the lumped parameters model, computing the new state at t^{n+1} of the circulatory network starting from the previous one (at t^n) and the pressure data given by the Navier-Stokes solver. In this way we compute the flow rates at the current time step $n+1$ that become boundary data for solving a flow rate Navier-Stokes problem (with the Lagrangian multiplier

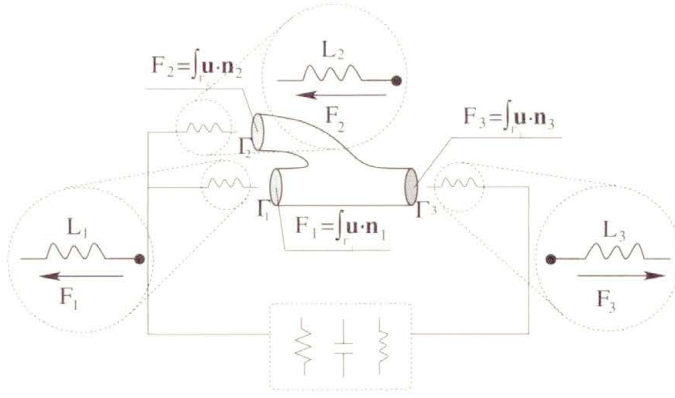

FIGURE 16. Scheme of coupling between the whole system and a local district where the bridging regions are given by inductors.

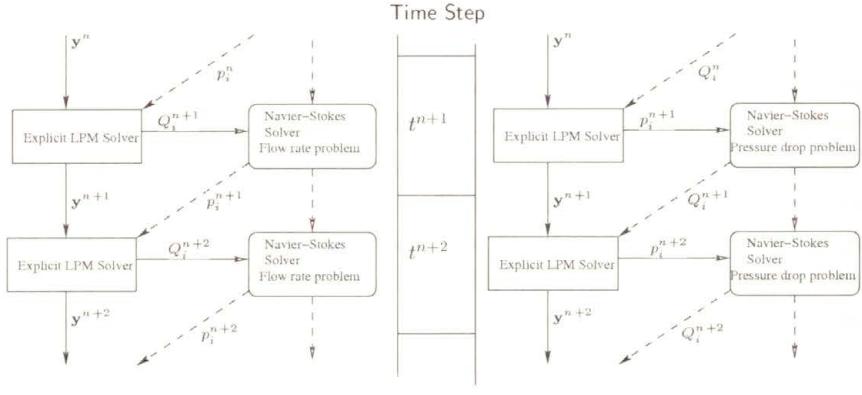

FIGURE 17. Possible numerical scheme for the coupling of a Lumped Parameter Model (LPM) and the Navier-Stokes problem: on the left the case corresponding to Fig. 16, on the right the one corresponding to Fig. 15.

approach). For solving the coupled problem of Fig. 15, the corresponding numerical scheme is in Fig. 17 right.

Numerical results and discussion about these methods can be found in [45], [50] and in [37]. In the latter work, in particular, the 3D compliant case is addressed, that requires specific interface conditions for the compliant vascular wall. We mention also an example of multiscale 3D-0D models proposed in [6], illustrating the relevance of the multiscale approach in the numerical simulation of the blood flow in a carotid bifurcation. CT scans of a stenosed carotid artery have been used for reconstructing a 3D geometry

both of a occluded and of a healthy (by modification of the original images) carotids. Numerical results have been obtained both for a stand-alone and a multiscale model (see Fig. 18) in the two geometries. The results outline the relevance of the description of the whole circulatory cerebral system in prescribing correct boundary conditions and definitely obtaining significant numerical results.

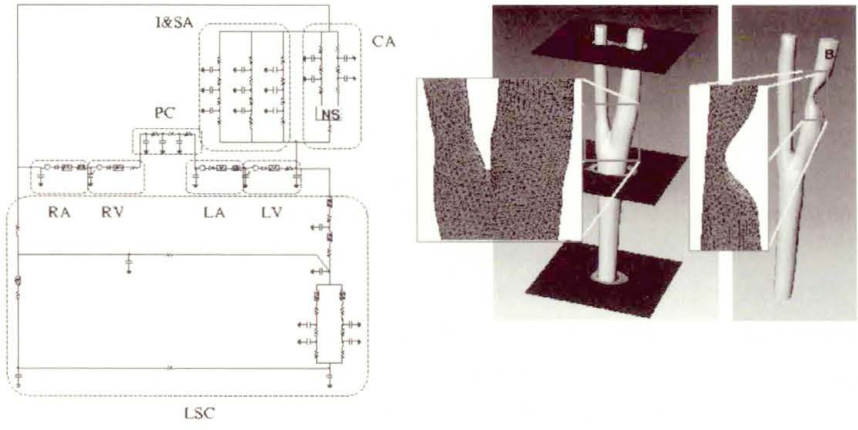

FIGURE 18. Left: Lumped parameter model for the multiscale carotid simulation. Right: Healthy and stenosed carotid model. Taken from [6].

Remark 3. In the last years, numerical methods for solving complex real problems in scientific computing by means of *domain decomposition methods* (DDM) have received great attention: as a recent reference, we quote [49]. The numerical approach to problems of increasing complexity quite naturally compell the identification of simpler "subproblems" that can be solved separately from the others, in order to setting up more effective numerical algorithms. Among the others possible examples, we quote fluid-structure interaction problems in hemodynamics, both at the mechanical and biochemical level (see [39, 51, 52, 69]).

In our framework, it is reasonable to assimilate the flux data to (mean) *Dirichlet* data, since they refer to the velocity field, while (mean) pressure data can be assimilate to *Neumann* condition, since they refer to the pressure, i.e. to the normal stress tensor which is a natural condition for the classical variational formulation of the Navier-Stokes equations. In this respect, the iterative algorithms presented above (and the ones that will be introduced for the 3D-1D coupling) can be considered an extension of the *Dirichlet-*

Neumann substructuring iterative method, widely adopted in the context of DDM. This link can provide suggestions for setting up some improvements in the algorithms, exploiting the theoretical framework of DDM.

5.2. Coupling 1D and 3D Models

Let us consider now the coupling of 3D and 1D models. Since we are still dealing with a reduced model, involving mean quantities and the pointwise Navier-Stokes model, we will have to handle "defective" data problems, according to the strategies illustrated in Sect. 4. In particular, as we have pointed out in the previous section, if we consider a compliant 3D domain, specific interface conditions will be needed by the differential problem associated to the vessel wall description in the 3D model. Moreover, the mathematical hyperbolic nature of 1D models will require a careful treatment of the interface conditions, based on a characteristics analysis (see Sect. 2). Since the 1D models are more accurate than the 0D ones, we have more possibilities in devising interface conditions. A priori, it is reasonable to look for the continuity of different quantities at the interface Γ_a, namely the flux, the mean pressure (or the total mean pressure), or the normal stresses or also the characteristic variables incoming to the 1D domains and, in the case of a compliant 3D domain, the interface area. The continuity of some of these quantities will be enough to force all the others: a complete discussion of the different possible interface conditions set is carried out in [15] and [16]. To these references the reader is referred (see also [1]) for some numerical results and examples.

Here we limit ourselves to point out that at the numerical level, the explicit coupling of 3D and 1D solver similar to the one illustrated for the 3D and 0D models can be affected by numerical instabilities, depending e.g. on the physical properties of the vascular walls. In these cases, we need to resort to an *implicit* coupling, achieved by iterating the computation of the 3D and the 1D problems at each time step, as it is illustrated in Fig. 19. In this scheme, we are supposing that the 1D model computes the pressure at the interface and the incoming characteristic variable W_1 is imposed at its inlet from the flow rate and the area computed by the 3D model. Relaxation parameters ε_1 and ε_2 can be tuned for improving the convergence of the scheme. A suitable stopping criterion will be adopted for ending the inner loop at each time step.

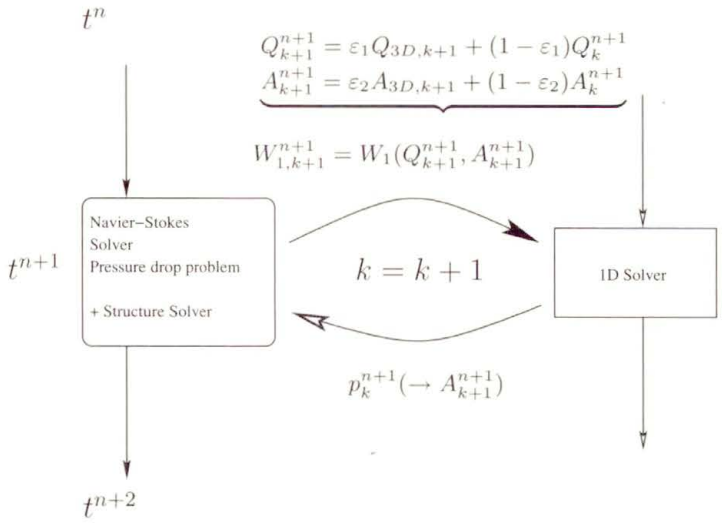

FIGURE 19. Implicit coupling of 3D and 1D solvers.

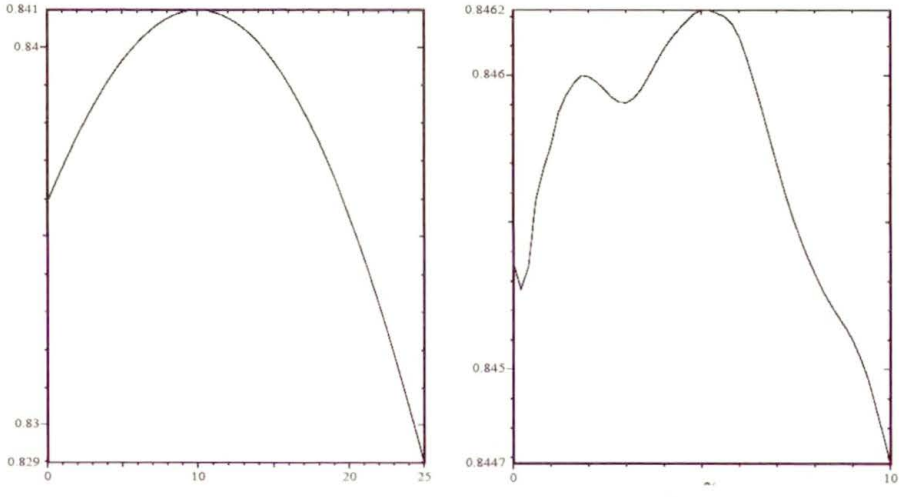

FIGURE 20. Left: Area in the upstream 1D model in the physiological case ($t = 0.016$ s); Right: Area in the upstream 1D model in the stented artery: observe the overload induced by the reflections due to the presence of the stent. Taken from [44].

In Fig. 20 (taken from [44]) we illustrate an example of the results obtained with this scheme in the numerical solution of a coupled 1D-3D-1D

model. The 3D model is supposed to be rigid. This can be regarded as the model of an artery with a stent, which is really stiffer than the physiological vascular tissue. In particular, it is possible to appreciate the overload in the proximal (=upstream with respect to the stent) 1D domain in the pressure, induced by the (physiological) reflections at the interface with the 3D stented model.

5.3. Coupling 0D and 1D Models

We finally consider the coupling of 1D and 0D models. Since we are actually coupling reduced models, both dealing with average (in space) quantities, we will not have defective boundary problems to solve. The crucial issues, in this case, are the boundary treatment of the 1D models, and the branching numerical treatment, addressed in Sect. 2.2.

The mathematical analysis of this class of heterogeneous problems can be carried out by means of fixed point techniques (see [18]) in a way similar to the one followed for the coupling of 3D and 0D models. See also [34]. The numerical solution can be in some cases obtained by coupling the discretized equations (in space and time for the 1D model, in time for the 0D one) in a monolithical solver. In general, it is however possible to resort to an iterative approach similar to the ones presented in the previous sections, in which a 1D and a 0D solvers are iteratively called in the multiscale numerical device.

The practical interest for this kind of models relies in the set up of systemic models for the description of the pressure wave propagation in the arterial tree (1D model) induced by the heart action (0D model), see [58], [19]. In particular, in [19] a 1D newtork including the largest 55 arteries (see Fig. 21 left) is coupled with the heart lumped parameter model given in Sect. 3.2 and a three elements Windkessel model for the peripheral circulation. The numerical coupling of the heart model and the 1D network has been obtained by following the scheme illustrated in Fig. 22. As a matter of fact, the two models are coupled only during the systolic phase, while in the diastolic one a null flux condition is imposed at the entrance of the aorta. The opening and closing of the aortic valve is driven by the comparison between the ventricular and the aortic pressure.

In Fig. 23 the relevance of the multiscale approach is clearly put in evidence: if the action of the heart is simply modelled by a prescribed boundary

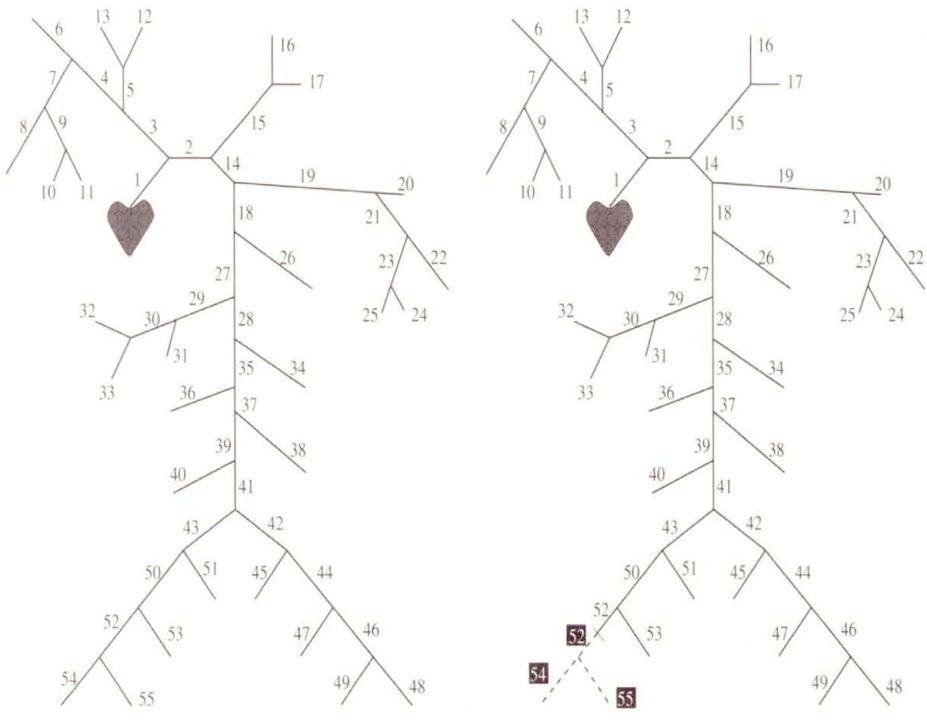

FIGURE 21. Arterial tree composed of a set of 55 straight vessels, described by 1D models (see [65]). On the right a pathological case, in which some of the vessel are supposed to be completely occluded.

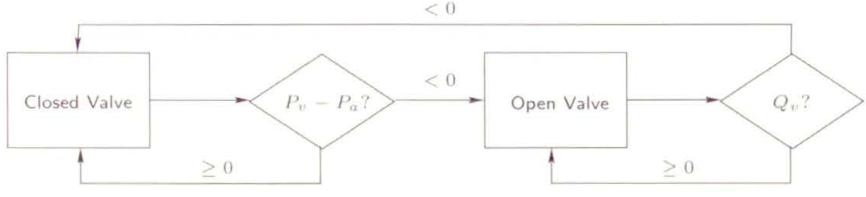

FIGURE 22. Flow chart representation of the aortic valve modeling.

condition at the inlet of the aorta (as it is usally done—left column), the results can be significantly different, with an underestimation of the heart overload due for instance to a pathological occlusion (dotted lines).

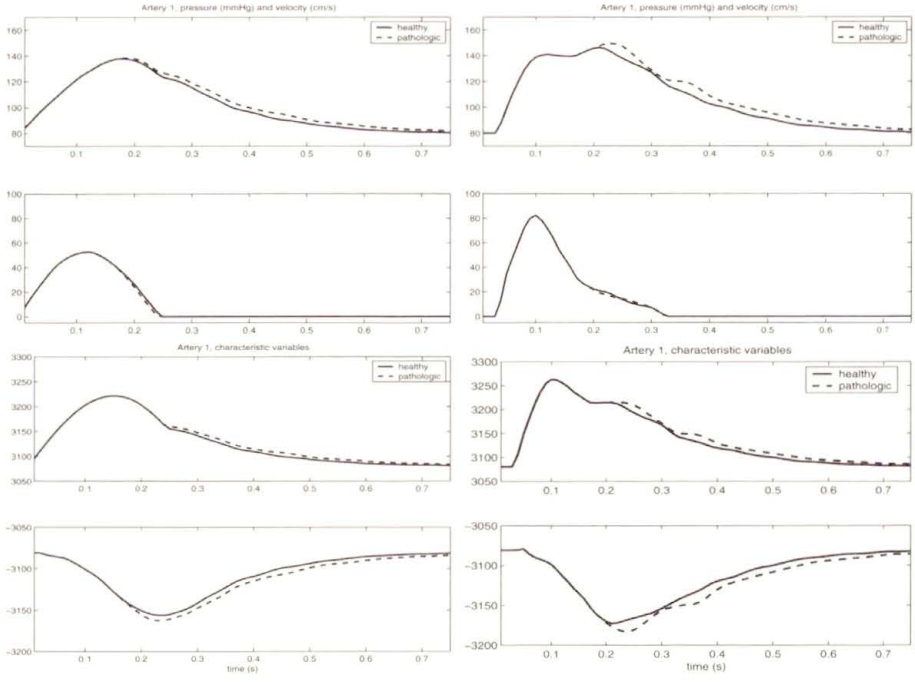

FIGURE 23. Comparison between the results obtained with standard proximal conditions (left) and the multiscale coupling with the ventricular model (right). Values of velocity and pressure in the mid-point of the aorta are presented in the first two rows. The last two rows illustrate a comparison between the Riemann invariants W_1 and W_2, respectively. Adult circulation in a physiologic (solid) and pathologic (dotted) test case are simulated.

6. Numerical Results in a Case of Clinical Interest

Numerical results obtained in more realistic contexts, still based on the approach of the present work, can be found in [31, 35, 36]. In these references the adoption of geometrical multiscale models has given good results for analysing, by means of numerical simulations, the dynamics of flow patterns in morphologically complex vascular districts in the context of paediatric surgery. The proposed methodology was in particular applied to a reconstructive procedure, used in cardiovascular paediatric surgery to treat a group of complex congenital malformations. There are different solutions for carrying out this kind of interventions (see [35, 36] and Fig. 24) and it is not easy, in general, to state which should be considered the best for the patient at hand. In the multiscale models adopted in this analysis, a 3D realistic morphology

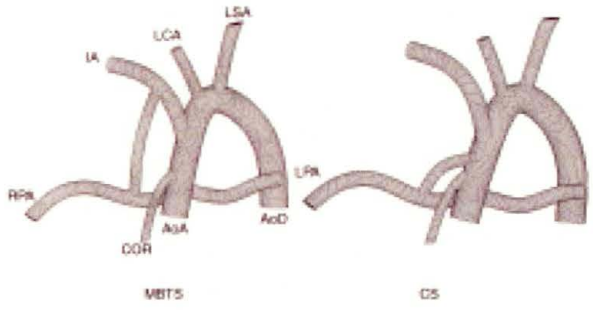

FIGURE 24. Two possible realizatons of the Norwood operation: Modified Blalock-Taussig shunt (left) and Central Shunt (right), from [35].

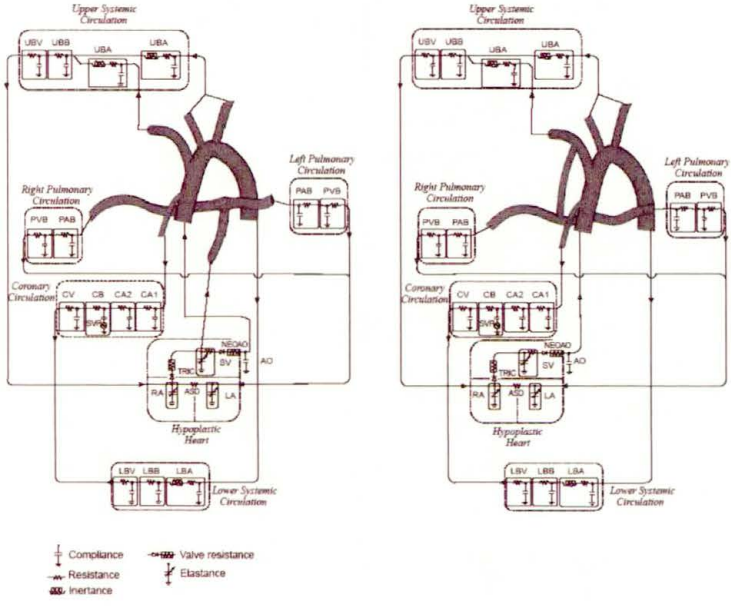

FIGURE 25. Multiscale model of the Modified Blalock Taussig Shunt (left) and of the right ventricle—pulmonary artery shunt or *Sano operation* (right, from [36]).

including the innominate artery, the pulmonary, carotid and subclavian arteries and the shunt are coupled to a lumped model composed by different blocks describing the rest of the pulmonary circulation, the upper and lower body, the aorta, the coronary system and the heart (see Fig. 25). Due to the complexity of the vascular 3D, the adoption of stand-alone classical fluid dynamics model failed to give accurate description of the velocity and pressure

fields (see [31]). With the adopted multiscale approach, i.e. using boundary conditions that account for the circulatory system, this was avoided and the inlet velocity profile reversal was correctly reproduced (In Fig. 25 and Fig. 26 we report some snapshots of the computed local solution). The prediction of both the local and the global haemodynamics after a surgical correction, leads to the quantification of pressure drops across the repaired region as well as to that of flow distribution into the major cardiovascular districts, which is an extremal important issue. Geometrical multiscale numerical modeling can help therefore the surgeon in the optimal choice of shunt size and placement.

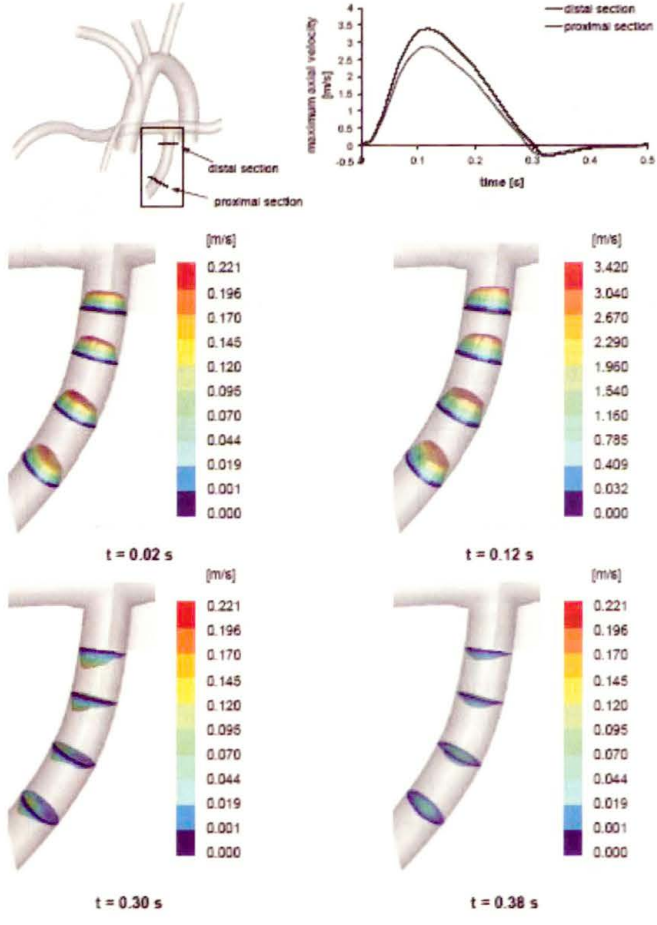

FIGURE 26. Velocity fields at different instants of the heart beat in the Sano operation (from [36]).

Acknowledgements

The authors wish to acknowledge all the people that, at various and different level, have collaborated to the results described in the report. In alphabetical order, Jean-Frederic Gerbeau, Daniele Lamponi, Vuk Milisic, Fabio Nobile, Tiziano Passerini, Alfio Quarteroni, Stefania Ragni, Simon Tweddle, Christian Vergara. They also acknowledge the collaboration with Gabriele Dubini and Francesco Migliavacca of the Laboratory of Biological Structures, Structural Engineering Department, Politecnico di Milano, and S. Sherwin and J. Peiro, Imperial College, London. This research would not have been possible without the support of various sponsoring agencies. In particular, the European Union, (through to the RTN Project "HaeMOdel"), the Italian "Ministero Università e Ricerca Scientifica e Tecnologica" and the "Fondazione Politecnico" and Siemens support of the Project ANEURISK (2005).

References

1. A. QUARTERONI and L. FORMAGGIA, *Mathematical Modelling and Numerical Simulation of the Cardiovascualr System*, [in:] N. Ayache [ed.] Computational Models for the Human Body, Elsevier, Amsterdam 2004.

2. M.E. BELIK, T.P. USYK, and A.D. MCCULLOCH, *Compuational Methods for Cardiac Electrophysiology*, [in:] N. Ayache [ed.] Computational Models for the Human Body, Elsevier, Amsterdam 2004.

3. L. FORMAGGIA and A. VENEZIANI, *Reduced and Multiscale Models for the Human Cardiovascular System*, MOX Rep. n.21, June 2003 (Von Karman Lecture Notes, 7^{th} Lecture Series on Biological Fluid Dynamics)

4. G. ALÌ , A. BARTEL, and M. GUNTHER, *Electrical RLC networks and diodes*, Technical Report RT237/01, Istituto per le Applicazioni del Calcolo "M. Picone", Italian National Research Council, `http://www.na.iac.cnr.it`, 2001.

5. J.P. ARCHIE and R.P. FELDTMAN, *Critical stenosis of the internal carotid artery*, Surgery, **89**:67–70, 1981.

6. R. BALOSSINO, F. MIGLIAVACCA, G. DUBINI, G. PENNATI, L. FORMAGGIA, M. TUVERI, and A. VENEZIANI, *Influence of boundary conditions on fluid dynamics in models of the cardiovascular system: a multiscale approach applied to the carotid bifurcation*, submitted to ASME J. Biomech. Eng., 2005.

7. A. BARNARD, W. HUNT, W. TIMLAKE, and E. VARLEY, *A theory of fluid flow in compliant tubes*, Biophys. J., **6**:717–724, 1966.

8. F. BREZZI and M. FORTIN, *Mixed and Hybrid Finite Elements*, SSCM n.5, Springer-Verlag 1991.

9. J. BRONZINO, [ed.] *The Biomedical Engineering Handbook*, chapter 157: Compartmental Models of Physiologic Systems, by C. Cobelli and M.P. Saccomani, pp.2375–2385, CRC Press, 1999.

10. J. BRONZINO, [ed.] *The Biomedical Engineering Handbook*, chapter 158: Cardiovascular Models and Control, by W.D. Timmons, pp.2386–2403, CRC Press, 1999.

11. W.R. DEAN, *The stream-line motion of fluid in a curved pipe*, Philos. mg. ser. 7, n.5, pp.673–695, 1928.

12. C. D'ANGELO, and V. MILISIC, *Reduced model for a coupling of axisymmetric Navier-Stokes equations with a reaction diffusion model for concentration*, submitted, available at the web site `iacs.epfl.ch`

13. G. D'ERRICO, A.ONORATI, and G.FERRARI, *An integrated 1d-2d fluid dynamic model for the predictions of unsteady flows in i.c. engine duct system*, [in:] IMECH In. Conf. "Computational and Experimental Methods in Reciprocating Engines", 2000.

14. J. DONEA, S. GIULIANI, H. LAVAL, and L. QUARTAPELLE, *Time-accurate solutions of advection-diffusion problems by finite elements*, Comp. Meth. Appl. Mech. Engng., **45**:123–145, 1984.

15. L.FORMAGGIA, J.F. GERBEAU, F. NOBILE, and A. QUARTERONI *On the coupling of 3d and 1d navier-stokes equations for flow problems in compliant vessels*, Comp. Math. Appl. Mech. Eng., **191**:561–582, 2001.

16. L.FORMAGGIA, J.F. GERBEAU, F. NOBILE, and A. QUARTERONI *Numerical treatment of defective boundary conditions for the Navier-Stokes equation*, SIAM J. Num. Anal., **40**(1):376–401, 2002.

17. D. LAMPONI, *One dimensional and multiscale for blood flow circulation*, PhD thesis, Thesis 3006, EPFL, Lausanne, 2004.

18. M.A. FENRANDEZ, V. MILISIC, and A. QUARTERONI, *Analysis of a geometrical multiscale blood flow model based on the coupling of ODE and Hyperbolic PDE's*, SIAM MMS, **4**:215–236, 2005.

19. L. FORMAGGIA, D. LAMPONI, M. TUVERI, and A. VENEZIANI, *Numerical modeling of a 1D arterial network coupled with a lumped parameter representation of the heart*, submitted, (available at the web site `mox.polimi.it`), 2005.

20. L. FORMAGGIA, D. LAMPONI, and A. QUARTERONI, *One dimensional models for blood flow in arteries*, J. Eng. Math. n.47, pp.251–276, 2003.

21. A.E. GREEN and P.M. NAGHDI, *A direct theory of viscous fluid in pipes. I. Basic general developments*, Phil. Trans. Royal Soc. London, 1993.

22. A.E. GREEN, P.M. NAGHDI, and M.J. STALLARD, *A direct theory of viscous fluid in pipes. I. Flow of incompressible viscous fluid in curved pipes*, Phil. Trans. Royal Soc. London, 1993.

23. R. GLOWINSKI and P.L. TALLEC, *Augmented Lagrangian and Operator Splitting Methods in Nonlinear Mechanics*, Studies in Applied Mathematics, SIAM, Philadelphia, 1989.

24. E. GODLEWSKI and P.-A. RAVIART, *Numerical Approximation of Hyperbolic Systems of Conservation Laws*, *Applied Mathematical Sciences*, **118**, Springer, New York 1998.

25. G. HEDSTROM, *Nonreflecting boundary conditions for nonlinear hyperbolic systems*, J. Comp. Physics, **30**:222–237, 1979.

26. J. HEYWOOD, R. RANNACHER, and S. TUREK, *Artificial Boundaries and Flux and Pressure Conditions for the Incompressible Navier–Stokes Equations*, Int. J. Num. Meth. Fluids, **22**:325–352, 1996.

27. F. HOPPENSTEADT and C. PESKIN, *Mathematics in Life Sciences and Medicine*, Springer-Verlag, New York 1992.

28. G. JAGER, N. WESTERHOF, and A. NOORDERGRAF, *Oscillatory flow impedance in electrical analog of the arterial system*, Circ. Res., **16**:121–133, 1965.

29. J. KEENER and J. SNEYD, *Mathematical Physiology* Springer-Verlag, New York 1998.

30. E. KRAUSE, *Modeling of the circulatory system*, Lecture Notes of the VKI Course on Fluid Dynamics and Biological Flow, Course 04-1998, 1998.

31. K. LAGANÀ, G. DUBINI, F. MIGLIAVACCA, R. PIETRABISSA, G. PENNATI, A. VENEZIANI, and A. QUARTERONI, *Multiscale modelling as a tool to prescribe realistic boundary conditions for the study of surgical procedures*, Biorheology, **39**:259–364, 2002.

32. R. LEVEQUE, *Numerical Methods for Conservation Laws*. Birkhauser, Basel 1990.

33. V. MARTIN, F. CLÉMENT, A. DECOENE, and J.F. GERBEAU *Parameter identification for a one-dimensional blood flow model*, to appear, ESAIM Proceedings, 2005.

34. V. MILISIC and A. QUARTERONI, *Analysis of lumped parameter models for blood flow simulations and their relation with 1D models*, M2AN, **28**:613–632, 2004.

35. K. LAGANA, R. BALOSSINO, F. MIGLIAVACCA, G. PENNATI, E.L. BOVE, M.R. DE LEVAL, and G. DUBINI, *Multiscale modeling of the cardiovascular system: application to the study of pulmonary and coronary perfusions in the univentricular circulation*, J. Biomech., **38**:1129–1141, 2005.

36. F. MIGLIAVACCA, R. BALOSSINO, G. PENNATI, G. DUBINI, T.Y. HSIAB, M.R. DE LEVAL, and E.L. BOVE, *Multiscale modelling in bio fluid dynamics: Application to reconstructive paediatric cardiac surgery*, J. Biomech, to appear, 2005.

37. A. MOURA and C. VERGARA, *Flow rate boundary conditions in compliant domains and applications to the multiscale modelling of the cardiovascular system*, in preparation, 2005.

38. W. NICHOLS and M. O'ROURKE, *Mc Donald's Blood Flow in Arteries*, Edward Arnold Ltd., Third edition, London 1990.

39. F. NOBILE, *Numerical approximation of fluid-structure interaction problems with applications to hemodynamics*, PhD th., École Polytèchnique Fèdèrale Lausanne, 2001.

40. A. NOORDERGRAAF, H. BOOM, and P. VERDOUW, *A human systemic analog computer, 1st Congr. Soc. Ballistocardiographic Res.*, p.23, A. Noordergraaf [ed.], 1960.

41. M.S. OLUFSEN and A. NADIM, *On deriving lumped models for blood flow and pressure in the systemic arteries*, Math. Biosc. and Eng., **1**(1) : 61–80, 2004.

42. M. OLUFSEN and J. OTTESEN, *A fluid dynamical model of the aorta with bifurcations*, Tekst 297, Rotskilde Univ., 1995.

43. T. PEDLEY, *The Fluid Mechanics of Large Blood Vessels*, Cambridge Univ. Press, Cambridge, 1980.

44. T. PASSERINI, *Multiscale Models for the Vascular System: Numerical Coupling of 3D and 1D models*, Degree Thesis in Biomedical Eng., Poltecnico di Milano [in italian; available at the web site `mox.polimi.it`], 2005.

45. A. QUARTERONI, S. RAGNI, and A. VENEZIANI, *Coupling between lumped and distributed models for blood flow problems*, Comp. Vis. Science, **4** : 111–124, 2001.

46. A. QUARTERONI, M. TUVERI, and A. VENEZIANI, *Computational vascular fluid dynamics: problems, models and methods*, Comp. Vis. Science, **2**(4) : 163–197, 2000.

47. A. QUARTERONI, R. SACCO, and F. SALERI, *Numerical Mathematics*, Springer-Verlag, New York 2002.

48. A. QUARTERONI and A. VALLI, *Numerical Approximation of Partial Differential Equations*, Springer Verlag Series in Computational Mathematics n.23, 1994.

49. A. QUARTERONI and A. VALLI, *Domain Decomposition Methods for Partial Differential Equations*, Oxford University Press, Oxford, 1999.

50. A. QUARTERONI and A. VENEZIANI, *Analysis of a geometrical multiscale model based on the coupling of ODE's and PDE's for blood flow simulations*, Mult. Mod. Simul., **1**(2) : 173–195, 2003.

51. A. QUARTERONI, A. VENEZIANI, and P. ZUNINO, *A domain decomposition method for advection-diffusion processes with application to blood solutes*, SIAM J. Sci. Comp., **23**(6) : 1959–1980, 2002.

52. A. QUARTERONI, A. VENEZIANI, and P. ZUNINO, *Mathematical and numerical modeling of solutes dynamics in blood flow and arterial wall*, SIAM J. Num. Anal., **39**(5) : 1488–1511, 2002.

53. V. RIDEOUT and D. DICK, *Difference-differential equations for fluid flow in distensible tubes*, IEEE Trans. Biomed. Eng., BME-**14**(3) : 171–177, 1967.

54. Y. SAAD, *Iterative Methods for Sparse Linear Systems*, PWS Publishing Company, Boston 1996.

55. K. SAGAWA, H. SUGA, and K. NAKAYAMA, *Instantaneous pressure-volume ratio of the left ventricle versus instantaneous force-length relation of papillary muscle*, [in:]

J. Baan, A. Noordergraaf, and J. Raines, [eds.], Cardiovascular System Dynamics, pp.99–105, 1978.

56. N. SMITH, A. PULLAN, and P. HUNTER, *An anatomically based model of coronary blood flow and myocardial mechanics*, SIAM J. Appl. Math., **62**(3) : 990–1018, 2003.

57. J. STETTLER, P. NIEDERER, and M. ANLIKER, *Theoretical analysis of arterial hemodynamics including the influence of bifurcations, part I: Mathematical model and prediction of normal pulse patterns*, Annals of Biomedical Engineering, **9** : 145–164, 1981.

58. F. MERENDA, N. STERGIOPULOS, *LV-arterial tree interaction and aortic waveforms: a varying elastance based study*, in preparation, 2005.

59. F. TORRENT-GUASP, *The Cardiac Muscle*, Juan March Foundation, Madrid, 1973.

60. K. THOMPSON, *Time dependent boundary conditions for hyperbolic systems*, J. Comp. Physics, **68** : 1–24, 1978.

61. A. VENEZIANI, *Boundary conditions for blood flow problems*, [in:] *Proc. ENUMATH97, Heidelberg*, R. Rannacher [ed.], pp.596–607

62. A. VENEZIANI and C. VERGARA, *Flow rate defective boundary conditions in haemodynamics simulations*, Int. J. Num. Meth. Fl., 2004.

63. A. VENEZIANI and C. VERGARA, *An approximate method for solving incompressible Navier-Stokes problem with flow rate conditions*, in preparation, 2005.

64. N. WESTERHOF, F. BOSMAN, C. VRIES, and A. NOORDERGRAAF, *Analog studies of the human systemic arterial tree*, J. Biomech., **2** : 121–143, 1969.

65. J.J. WANG, and K. PARKER, *Wave propagation in a model for arterial circulation.*, J. Biomech., **37** : 457–470, 2004.

66. M. ZACEK and E. KRAUSE, *Numerical simulation of the blood flow in the human cardiovascular system*, J. Biomech., **29**(1) : 13–20, 1996.

67. S. VELE and U. VILLA, *1D Models for blood dynamics and solutes*, [in italian], Degree Thesis, Politecnico di Milano, available at the web site `mox.polimi.it`

68. C. ZARINS, *Hemodynamics in atherogenesis*, [in:] W. Moore, [ed.], Vascular Surgery. A Comprehensive Review, pp.86–96. W.B. Saunders, Philadelphia, PA, 1991.

69. P. ZUNINO, *Mathematical and numerical modeling of mass tranfer in the Vascular System*, PhD thesis, Ècole Polytèchnique Fèdèrale Lausanne, 2002.